

# Trauma-Responsive Scaffold Synchronizing Oncolysis Immunization and Inflammation Alleviation for Post-Operative Suppression of Cancer Metastasis

Junlin Li, Ping Zhang, Minglu Zhou, Chendong Liu, Yuan Huang,\* and Lian Li\*



Cite This: <https://doi.org/10.1021/acsnano.1c11562>



Read Online

ACCESS |



Metrics & More



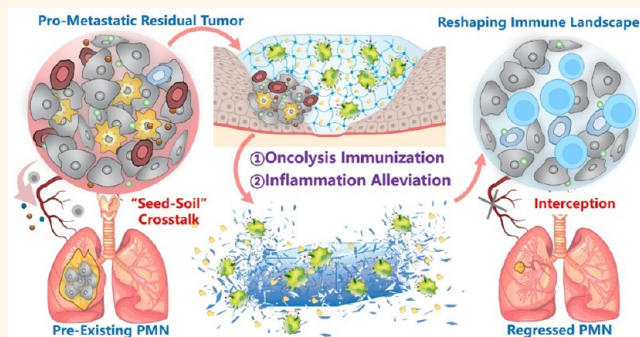
Article Recommendations



Supporting Information

**ABSTRACT:** Tumor surgery can create an inflammatory trauma to aggravate residual tumor “seed” to colonize pre-metastatic niches (PMNs) “soil” at secondary sites, thereby promoting post-operative metastasis. However, two-pronged strategies for post-surgical elimination of asynchronous “seeds” and “soil” at different regions are currently lacking. Here, we have designed a hydrogel that can be injected into a resection cavity, where it immediately forms a scaffold and gradually degrades responding to enriched reactive oxygen species at adjacent trauma for local delivery and on-demand release of autologous cancer cells succumbing to oncolysis (ACCO) and anti-inflammatory agent. The autologous cell source self-provides a whole array of tumor-associated antigens, and the oncolysis orchestration of a subcellular cascade confers a self-adjuvanting property, together guaranteeing high immunogenicity of the ACCO vaccine that enables specific antitumor immunization. In parallel, inflammation alleviation exerted bidirectional functions to reshape the local immune landscape and resuscitate ACCO, leading to the eradication of residual tumor “seeds” while simultaneously intercepting the “seed–soil” crosstalk to normalize distant lung leading to regression of pre-existing PMN “soil”. As a result, regional and metastatic recurrence were completely thwarted. Together, this framework synchronizing oncolysis immunization and inflammation alleviation provides an effective option for post-operative suppression of metastasis.

**KEYWORDS:** post-operative metastasis, hydrogel, oncolysis, cell vaccine, pre-metastatic niche



Despite the fact that less than 10% of breast cancer are *de novo* metastatic, metastatic recurrence after surgical resection exceeds 30%, highlighting that surgery has the risk of promoting metastasis.<sup>1,2</sup> The underlying causes are multifactorial but largely ascribed to two factors: (1) surgical stress-induced change in local trauma that mobilizes residual tumor cell “seeds”,<sup>3,4</sup> and (2) pre-metastatic niche (PMN) already established in distant site that persists to create fertile “soil” for subsequent metastasis even after resection.<sup>5,6</sup> Although separate efforts to ameliorate post-surgical micro-environment or disrupt PMN formation have been made and judiciously reviewed,<sup>3,6</sup> metastasis after surgery of breast cancer remains an unresolved clinical problem that bodes poorly for survival. Because post-surgical evolution of the seeds and soil at different regions are dynamic and asynchronous,<sup>7</sup> long-lasting and two-pronged strategies that simultaneously reshape the

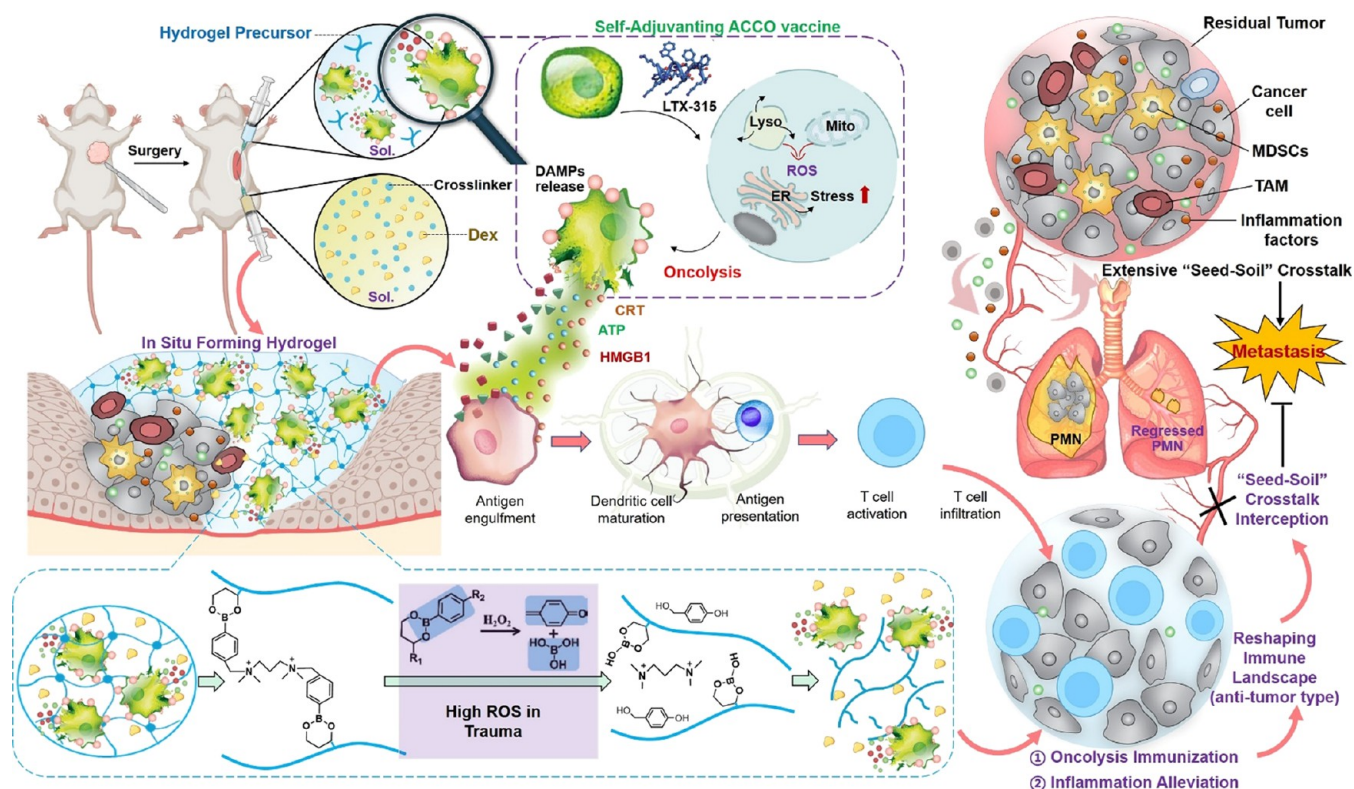
residual tumor and regress the pre-existing PMN are necessary but currently lacking.

Along with abrogation of metastasis-promoting effects, the elimination of residual tumor is equally important for post-operative suppression of metastasis.<sup>8,9</sup> Newly developed immunotherapies can train an immune system to identify and eradicate tumor cells while sparing normal tissues.<sup>10–12</sup> Local administration of oncolytic virus to infect and lyse cancer cells can initiate tumor oncolysis, which can elicit an antitumor

**Received:** December 28, 2021

**Accepted:** March 22, 2022

### Scheme 1. Strategy Illustration of Synchronizing Oncolysis Immunization and Inflammation Alleviation to Intercept Seed–Soil Crosstalk for Post-Operative Suppression of Cancer Metastasis



response through the release of adjuvant danger-associated molecular patterns (DAMPs) and subsequent recruitment of immune effectors.<sup>13,14</sup> Oncolytic virotherapy is now emerging as an expanding research area and a powerful immunostimulatory strategy against transdermally accessible tumors (e.g., breast cancer) but is only subject to intratumoral injection.<sup>15</sup> Similar with other immune-directed therapies blocking immune checkpoint or inducing immunogenic cell death (ICD),<sup>16</sup> virotherapy faces several hurdles that impede its application in post-operative intervention. First, residual tumors after incomplete resection are microscopic, sporadically scattered at adjacent tissues, and generally inaccessible by the desired amount of oncolytic virus; Second, virotherapy requires the presence of a primary tumor to generate antigen-specific T cell responses, but surgery resects the majority of tumor tissues with insufficient antigen sources left; Third, immunosuppression is exacerbated in the surgery bed, thus rendering the immunotherapy less effective.<sup>3</sup>

Regarding the aforementioned issues, an autologous tumor cell vaccine may be an option well-suited to post-surgical management, since it self-provides a full set of tumor-associated patient-specific antigen epitopes.<sup>17,18</sup> Indeed, such a consideration has given rise to innovative attempts of developing a hydrogel matrix that encapsulates photosensitizer-loaded or coated cancer cells from resected tumors. After irradiation following the implantation in the surgical bed, the autologous tumor cells were transformed into an immunogenic vaccine and elicited a specific response against residual microtumors for personalized therapy.<sup>19,20</sup> Inspired by this, instead of turning tumors into a vaccine by inducing onsite oncolysis, we proposed to take one step ahead of current oncolytic therapy by locally delivering autologous cancer cells

succumbing to oncolysis (ACCO) as an antitumor vaccine. Whether ACCO can function as effective post-surgical cancer vaccine, guaranteeing both antigenicity and adjuvanticity, has been not yet reported. In addition, since extended release of immunotherapeutic locally at tumor-resection site enables sustainable stimulation,<sup>21</sup> a trauma-responsive scaffold that supports on-demand release of ACCO is needed. Moreover, combinatory approach capable of immunosuppression reversal and metastasis suppression is imperative as well.<sup>22</sup>

In this study, we have designed a trauma-inflammation-responsive and alleviating hydrogel scaffold for the local delivery of ACCO vaccine to suppress post-operative metastasis (Scheme 1). Immunogenic ACCO, with the whole array of tumor antigens and self-adjuncting property, is produced by a method of nonviral oncolysis that elicits a defined type of cell stress to orchestrate a subcellular cascade leading to substantial DAMP exposure. The hydrogel depot harboring ACCO can be *in situ* formed immediately after syringeable injection, creating a temporary shelter for antigens within local areas, and facilitates continuous immune activation, leading to a durable antigen-specific response against autologous tumor. We have also identified that the exacerbated inflammation inevitably induced by surgical stress as a multirole trigger to consolidate immunosuppression and maintain pro-metastatic “seed–soil” crosstalk. Hence, dexamethasone (Dex) was coloaded into the same hydrogel that could respond to an elevated level of reactive oxygen (ROS) in inflammatory trauma, allowing for on-demand drug release at the surgical resection site. As a result, inflammation alleviation exerted bidirectional functions to prime the local immune landscape and amplify the ACCO, leading to the eradication of residual tumor seeds while simultaneously intercepting the seed–soil crosstalk to normal-



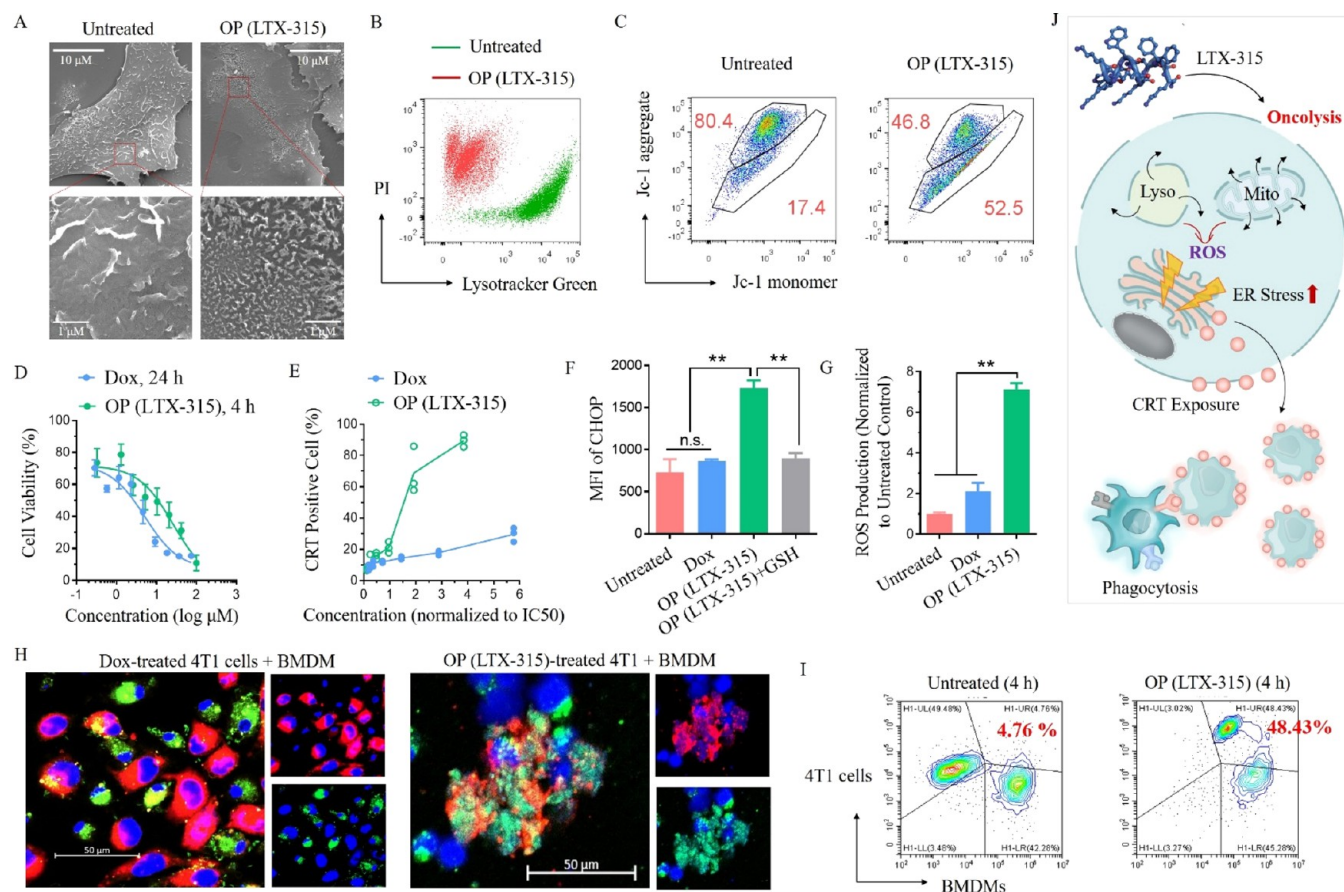


**Figure 1.** Oncolysis amplifies immunogenicity. (A) SEM images of tumor cell membrane, (B) flow cytometry analysis of the cell surface destruction and intracellular lysosome rupture, and (C) depolarization of mitochondrial membrane potential ( $\Delta\Psi_m = \text{Jc-1 aggregate/monomer}$ ) after treatment with OP. (D) Equivalent cytotoxicity achieved by treating 4T1 cells with a series of concentrations of either Dox for 24 h or OP for 4 h. *In vitro* measurement of (E) CRT exposure, (F) ER stress, and (G) intracellular ROS production after treatment with Dox or OP. Data are mean  $\pm$  s.d.,  $n = 3$  per group. Statistical analysis was performed using one-way ANOVA;  $**p < 0.01$ . (H) Confocal imaging and (I) flow cytometry analysis of phagocytosis of OP-treated DiO-labeled 4T1 cells (red) by DiR-labeled BMDMs (green) *in vitro*. (J) Illustration of OP-mediated oncolysis initiating a subcellular cascade to expose adjuvant CRT, an “eat me” signal.

ize distant lung leading to the regression of PMN soil and inhibition of metastasis. Together, these findings establish the coordination of (1) oncolysis immunization to eliminate recurrent tumors, and (2) complementary inflammation alleviation to reverse pro-metastatic influence as an effective strategy against post-operative metastasis.

## RESULTS AND DISCUSSION

**Characterization of ACCO as Self-Adjuvanting Vaccine.** Autologous cell-derived vaccine has the advantage of possessing abundance and breadth of an antigen source.<sup>17,18</sup> However, a low immunogenicity of autologous cell derivatives represents a huge challenge, which requires the codelivery of adjuvants or immunostimulants.<sup>23</sup> Here, to confer the self-adjuvanting attribute, oncolysis was induced in autologous cells by treating with LTX-315, an oncolytic peptide (OP) that closely mimicked oncolytic virus by recapitulating its cationic and amphipathic nature.<sup>24,25</sup>

We first confirmed the membranolytic mode of action for OP (LTX-315) in murine breast cancer (4T1) cells. Scanning electron microscopy (SEM) revealed severe membrane lysis and abundant perforations on the surface of OP-treated cells, with a considerably different morphology from untreated cells that had intact membranes with rich microvilli (Figure 1A).

Flow cytometry analysis also showed that, after OP exposure, the fluorescence of propidium iodide (PI, a membrane-impermeable dye) increased while the intensity of Lysotracker Green (lysosomal pH probe) decreased (Figure 1B), suggesting that OP disrupted both cellular and lysosomal membranes. Furthermore, OP also acted on mitochondrial membrane as evidenced by the depolarization of mitochondria membrane potential (Figure 1C). Collectively, OP exerted strong tropism for interacting with numerous biomembranes in 4T1 cells, which was a typical phenomenon for cells undergoing oncolysis.

Having demonstrated that OP triggered oncolysis in 4T1 cells, we next investigated whether oncolysis could endow ACCO with self-adjuvanting properties by exposing adjuvant calreticulin (CRT), one of the major hallmarks for ICD-associated DAMPs.<sup>16</sup> Because the anthracycline doxorubicin (Dox) was among a few cytotoxic drugs that could induce ICD as collateral effect, it has frequently been used to promote tumor immunogenicity for numerous immunochemotherapies.<sup>26,27</sup> Therefore, Dox was selected here as the control. As shown in Figure 1D, OP treatment for 4 h ( $\text{IC}_{50}$ , 9.17  $\mu\text{M}$ ) and Dox treatment for 24 h ( $\text{IC}_{50}$ , 3.47  $\mu\text{M}$ ) had comparable cytotoxicity within the same magnitude order. Moreover, the percentage of cells that had surface CRT exposure could reach

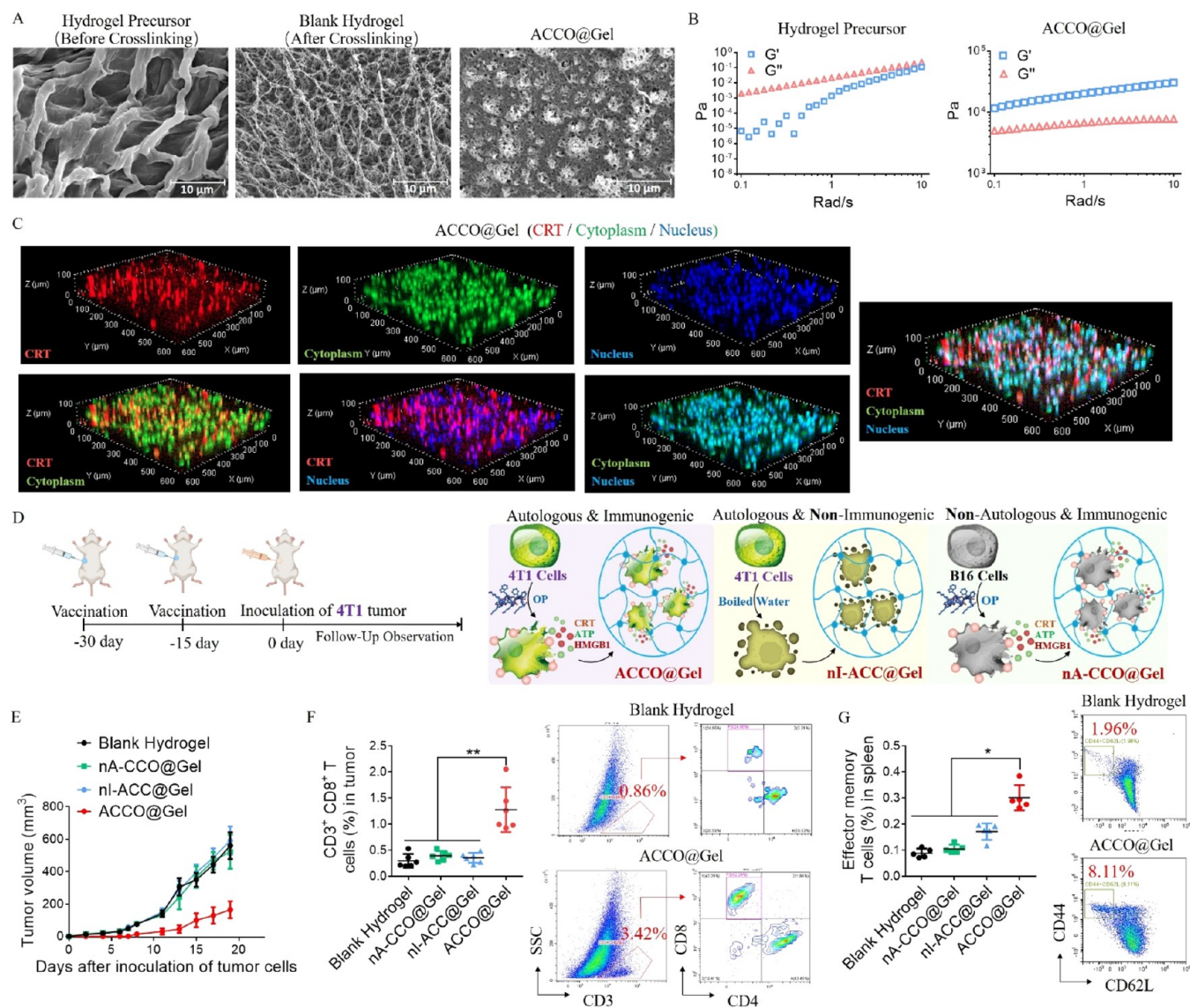


**Figure 2.** ACCO@Gel elicits antigen-specific immune memory. (A) SEM imaging and (B) frequency-dependent rheological properties of ACCO@Gel. (C) Three-dimensional construction images of ACCO@Gel. CRT (red), cytoplasm (green), and nucleus (blue) of ACCO were pre-stained before loading into the hydrogel. (D) Illustration of vaccination schedule and various cell-based hydrogel vaccines. (E) Tumor growth curves in mice after various vaccinations ( $n = 6$ ). Quantification and representative flow cytometry plots of (F) tumor-infiltrating CD3<sup>+</sup> T cells (gated on CD3<sup>+</sup> T cells) and (G) splenic CD44<sup>+</sup>CD62L<sup>-</sup> memory effector cells (gated on CD3<sup>+</sup> T cells) isolated from vaccinated mice at the end point ( $n = 6$ ). Data are mean  $\pm$  s.d. Statistical analysis was performed using one-way ANOVA; \* $p < 0.05$ , \*\* $p < 0.01$ .

over 80% within 4 h in response to OP, while approximately 40% CRT-positive cells at maximum was generated 24 h after Dox treatment (Figure 1E). This indicated that OP-induced oncolysis could be achieved at a substantially higher degree of ICD at an accelerated rate, which may be beneficial to shorten the interval between the acquisition of more immunogenic autologous cell sources and a post-operative vaccination. Since CRT exposure originates from the stress elevation in endoplasmic reticulum (ER),<sup>12</sup> the underlying mechanism could be ascribed to our finding that OP caused significant ER stress as indicated by the increment in the expression of C/EBP homologous protein (CHOP). Additional experimentation showed that OP did not directly induce ER stress but through ROS mediation, because such an effect could be attenuated in the presence of glutathione (GSH) as a ROS scavenger (Figure 1F). Indeed, OP could spur an exceedingly

high production of intracellular ROS (Figure 1G), probably owing to its capability to rupture lysosomes and damage mitochondria.<sup>24,28</sup> Meanwhile, the impact of Dox on ROS generation and ER stress induction was limited.

As a result of increased surface CRT functioning as an “eat me” signal,<sup>29,30</sup> substantial phagocytosis of OP-treated 4T1 cells by bone-marrow derived macrophages (BMDMs) was observed. By comparison, apparently less interaction occurred between untreated/Dox-treated cells and BMDMs (Figure 1H and Figure S1). In addition, flow cytometry analysis further confirmed that a majority of cells succumbing to oncolysis could be recognized and phagocytosed for potential antigen presentation (Figure 1I and Figure S1).

The above findings gave a clear picture (Figure 1J) that OP-mediated oncolysis potentially orchestrated a prograded cascade of subcellular membrane disruption  $\rightarrow$  ROS overproduction  $\rightarrow$



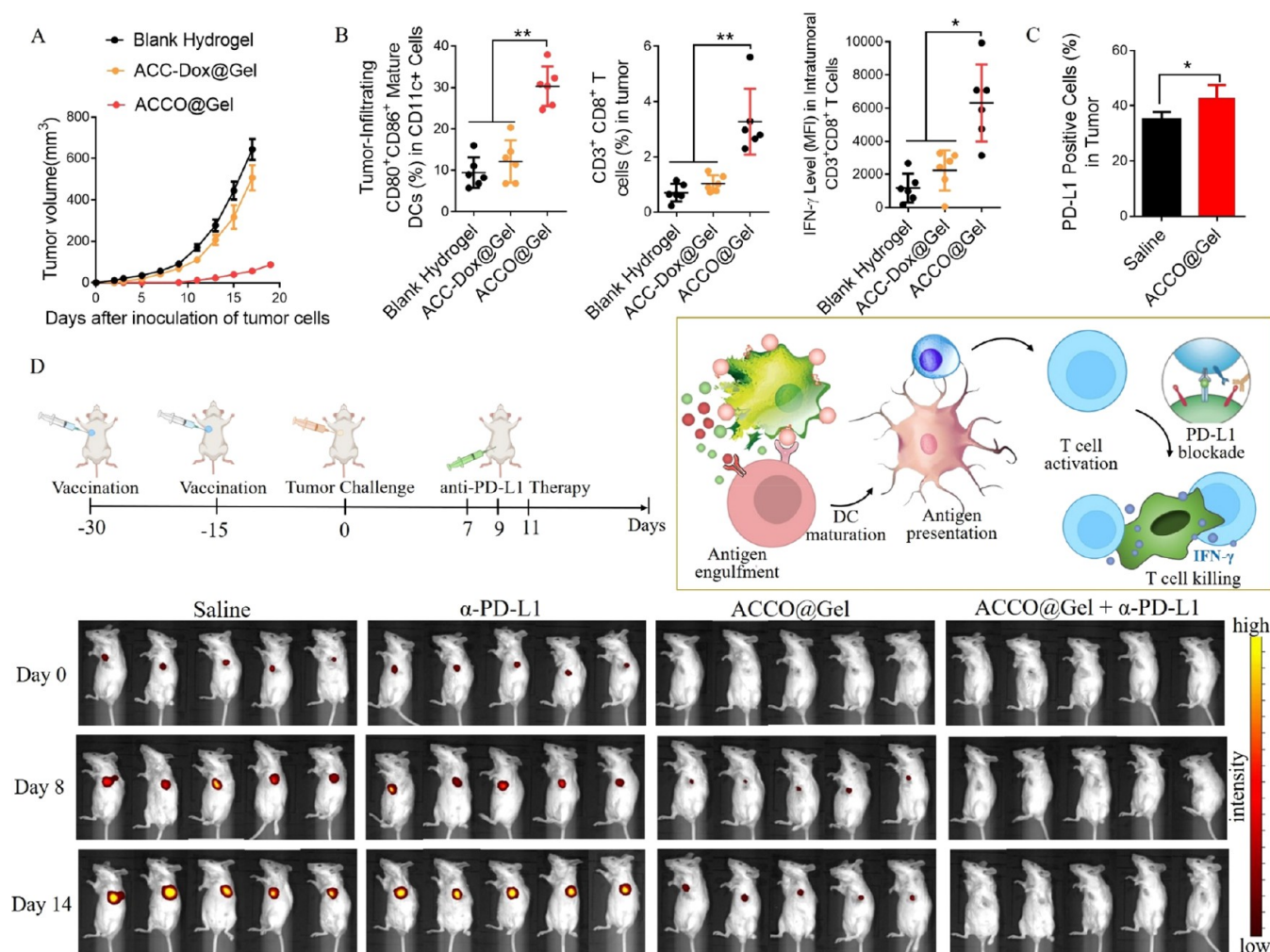


**Figure 3.** ACCO@Gel potentiates anti-PD-L1 therapy. (A) Tumor growth in vaccinated mice after inoculation of 4T1 tumor cells ( $n = 6$ ). (B) Frequencies of tumor-infiltrating CD80<sup>+</sup>CD86<sup>+</sup>CD11c<sup>+</sup> mature DCs and CD3<sup>+</sup>CD8<sup>+</sup> T cells, IFN- $\gamma$  level in intratumoral CD3<sup>+</sup>CD8<sup>+</sup> T cells, and (C) intratumoral PD-L1 expression in vaccinated mice at the end point ( $n = 6$ ). (D) *In vivo* representative bioluminescence imaging of 4T1-Luc-inoculated mice receiving combination of ACCO@Gel vaccination and anti-PD-L1 treatment as arrow indicated ( $n = 6$ ). Data are mean  $\pm$  s.d.,  $n = 6$  mice per group. Statistical analysis was performed using one-way ANOVA; \* $p < 0.05$ , \*\* $p < 0.01$ .

abnormal ER stress  $\rightarrow$  translocation of CRT from ER to cell surface  $\rightarrow$  immune phagocytosis, thereby evoking more profound ICD than the ICD that was induced collaterally and insufficiently by commonly used anthracycline. These results suggested the superiority of ACCO as highly immunogenic sources for a cancer vaccine.

**Validation of ACCO@Gel-Induced Immunization.** To extend the exposure of immunogenic ACCO, an injectable hydrogel<sup>31,32</sup> that could form a scaffold *in situ* was applied to load and controllably release ACCO. The scaffold, denoted as ACCO@Gel, was immediately assembled after the mixture of two syringeable solutions of the cross-linker (N1-(4-boronobenzyl)-N3-(4-boronophenyl)-N1,N1,N3,N3-tetramethylpropane-1,3-diaminium) and ACCO-containing hydrogel precursor poly(vinyl alcohol) (PVA). The cross-linker has dual phenylboronic acids that can spontaneously and rapidly react with diols on PVA to form ROS-labile pinacol ester. The microstructures of hydrogel scaffolds were then characterized using SEM after sublimation of frozen water by lyophilization (Figure 2A). Blank hydrogel after cross-linking showed an organized texture of polymer network with more elaborate and abundant pores or channels formed, which was distinctly

different from unassembled hydrogel precursor without cross-linking. For ACCO@Gel, cell payloads were compactly packed fitting in the porous structures of a hydrogel. Meanwhile, the hydrogel precursor showed a typical rheology of solution, while storage modulus ( $G'$ ) increased dramatically and exceeded loss modulus ( $G''$ ) for ACCO@Gel after a mixture of cross-linker solution and hydrogel precursor solution, thus further confirming that cross-linking led to sol-to-gel phase transition (Figure 2B). Then, the viscoelastic property of ACCO@Gel was studied. Strain sweep measurement (Figure S2A) showed that ACCO@Gel displayed a linear viscoelastic region ( $G' > G''$ ) with the oscillation strain ranging from 0.1% to 10%, indicating that the elastic property of the hydrogel was dominant with high stability in this region. Above 10% strain,  $G'$  decreased sharply while  $G''$  decreased gradually, indicating that the internal network of the hydrogel is gradually damaged. In addition, the compression and tension curves (Figure S2B) showed that ACCO@Gel had an apparent tendency to recover when withstanding a high compression, suggesting that ACCO@Gel is not fragile or easy to break down. Afterward, the tissue adhesiveness of ACCO@Gel was assessed using porcine skin as the substrate. Both tensile adhesion test (Figure

S2C) and shear adhesion tests (Figure S2D) were applied. As compared with the hydrogel precursor of PVA solution whose adhesiveness was too low to be determined, ACCO@Gel had apparent adhesive capacity to porcine skin, with tensile and shear adhesion strengths of  $\sim 5.8$  and  $\sim 56$  kPa, respectively. Similar with other studies<sup>32,33</sup> that utilized a PVA-based hydrogel for local drug delivery and biomedical purposes, we have also observed that the hydrogel scaffold could be peritumorally formed after *in situ* injection and adhere to the surrounding tissues of residual tumor after 4 days post tumor resection (Figure S2E).

Uniform and ordered dispersion of the cell nucleus, cytoplasm, and oncolysis-induced CRT exposure in ACCO@Gel was observed by three-dimensional scanning using confocal laser scanning microscopy, suggesting that the hydrogel matrix could effectively maintain abundant antigen sources and adjuvant DAMPs (Figure 2C).

We next evaluated the capability of ACCO@Gel to vaccinate mice against the subsequent challenge of a 4T1 murine breast tumor. Prior to vaccination assay, several cell-based hydrogel vaccines (Figure 2D) were prepared with cell sources derived from (i) ACCO (ACCO@Gel), (ii) non-immunogenic autologous cancer cell (nI-ACC@Gel), and (iii) nonautologous cancer cells succumbing to oncolysis (nA-CCO@Gel).

To fabricate ACCO@Gel, 4T1 cells were consecutively treated with OP and encapsulated into the hydrogel as described above. As expected, multiple DAMP-associated signals including surface-exposed CRT, extracellular ATP, and high mobility group box 1 (HMGB1) were vigorously provoked in response to OP-mediated oncolysis (Figure S3A). To fabricate nI-ACC@Gel, nonimmunogenic dead cells were loaded into the hydrogel after the incubation of 4T1 cells with boiled water (BW), which elicited minimal CRT exposure and ATP release (Figure S3A). In addition, nA-CCO@Gel was fabricated by treating nonrelevant B16 murine melanoma cells with OP following gelation. As evidenced by dramatic increase in the expression of surface CRT and secretions of ATP and HMGB1, OP converted B16 cells into an immunogenic vaccine as well (Figure S3B).

Afterward, mice were subject to two doses of vaccination before orthotopically inoculation of 4T1 breast cancer cells. As shown in Figure S4, no loss in body weight was observed in mice that received subcutaneous injection of various hydrogel vaccines. Meanwhile, histology analysis on major organs of healthy mice receiving various treatments showed no pathological abnormality in heart, liver, spleen, lung, and kidney (Figure S5), indicating no obvious toxicity systemically. Notably, as compared with a blank hydrogel, vaccination with nI-ACC@Gel or nA-CCO@Gel had no impact on inhibiting the growth of 4T1 tumors, while vaccination with ACCO@Gel significantly slowed the tumor progression (Figure 2E). It was worth noting that local administration with ACCO suspension failed to have the same promising effect as exerted by ACCO@Gel (Figure S6), highlighting the advantage of using a scaffold depot to encapsulate ACCO.

Immunology analysis at the end point showed that 4T1 tumors in the ACCO@Gel-vaccinated mice were infiltrated with a considerably higher frequency of CD8<sup>+</sup> T cells than those of the blank hydrogel pre-treated mice. Meanwhile, none of the vaccinations with nI-ACC@Gel or nA-CCO@Gel increased the number of tumor-infiltrating CD8<sup>+</sup> T cells beyond the basal level (Figure 2F). Moreover, ACCO@Gel

vaccination significantly expanded splenic CD44<sup>+</sup>CD62L<sup>-</sup> memory effector CD8<sup>+</sup> T cells, revealing the establishment of durable immunity, whereas such effects from nI-ACC@Gel and nA-CCO@Gel vaccination were limited (Figure 2G). These results emphasized (i) a tumor-specific antigen source and (ii) the acquisition of adjuvant immunogenicity as two dispensable factors for an effective cancer vaccine,<sup>17</sup> and such attributes empowered ACCO@Gel to elicit a long-term antitumor antigen-specific immune memory *in vivo*.

In another individual experiment following the same vaccination procedure as above, ACCO@Gel generated a reproducible outcome with a delay of tumor establishment and a dramatic inhibition of growth rate (Figure 3A). By comparison, the vaccination efficacy was moderate for ACC-Dox@Gel, which was derived from Dox-treated 4T1 cells. This result could be ascribed to the fact that ACCO with oncolysis-magnified immunogenicity was more readily phagocytosed by immune effector cells than Dox-treated cells (Figure 1). Indeed, vaccination with ACCO@Gel initiated a domino effect with a higher recruitment of mature dendritic cells (CD80<sup>+</sup>CD86<sup>+</sup>CD11c<sup>+</sup>) and infiltration of cancer cell-reactive T cells (IFN- $\gamma$ <sup>+</sup>CD8<sup>+</sup>) in orthotopic 4T1 tumors than vaccination with either blank hydrogel or ACC-Dox@Gel (Figure 3B).

Despite enhanced immunity against tumor challenge, ACCO@Gel failed to completely prevent the occurrence of tumor establishment, probably due to a high level of intratumoral PD-L1 that facilitated the evasion of 4T1 cells from T-cell-mediated immunosurveillance. Worst still, tumors after ACCO@Gel vaccination even slightly enhanced PD-L1 expression (Figure 3C), which was likely the result of increased IFN- $\gamma$ <sup>+</sup> that could induce PD-L1 upregulation as immunosuppressive feedback.<sup>29,34</sup> Therefore, we sought to improve the regimen by combining anti-PD-L1 therapy. As shown in Figure 3D, mice were orthotopically challenged with luciferase-expressing 4T1 breast cancer cells following two doses of ACCO@Gel vaccination and then treated with three doses of  $\alpha$ -PD-L1 monoclonal antibody to combat tumor onset. A bioluminescence imaging method was used to monitor the tumor progression. As compared with the saline-treated control, mice bearing 4T1 tumors did not respond to  $\alpha$ -PD-L1 alone. This could be explained by the immunogenically “cold” status in 4T1 tumors devoid of pre-existing T cells.<sup>35</sup> Meanwhile, vaccination with ACCO@Gel effectively expanded tumor-infiltrating T cells but only limited the tumors to relatively small volumes. Notably, consecutive treatments with ACCO@Gel vaccination and anti-PD-L1 therapy completely eradicated tumors (Figure 3D and Figure S7) because of their complementary functions to recruit and unleash tumor-reactive T cells. Together, these results revealed great capacity of the ACCO@Gel vaccine to elicit strong antitumor immunity.

**Trauma-Responsive Drug Release.** Because the efficacy of ACCO may compromise in inflammatory trauma, we further coloaded ACCO and anti-inflammatory Dex within one scaffold for post-surgical intervention. The scaffold platform was prepared with a similar procedure of mixing two injectable solutions of hydrogel precursor and ROS-labile cross-linker containing ACCO and Dex, respectively, to fabricate (ACCO+Dex)@Gel. To further confirm the necessity of ROS responsiveness for post-surgical practice of (ACCO+Dex)@Gel, we revealed that, as compared with pre-surgical tumors, post-surgical tumors significantly elevated intratumoral concentrations of H<sub>2</sub>O<sub>2</sub> (Figure 4A), which was due to the



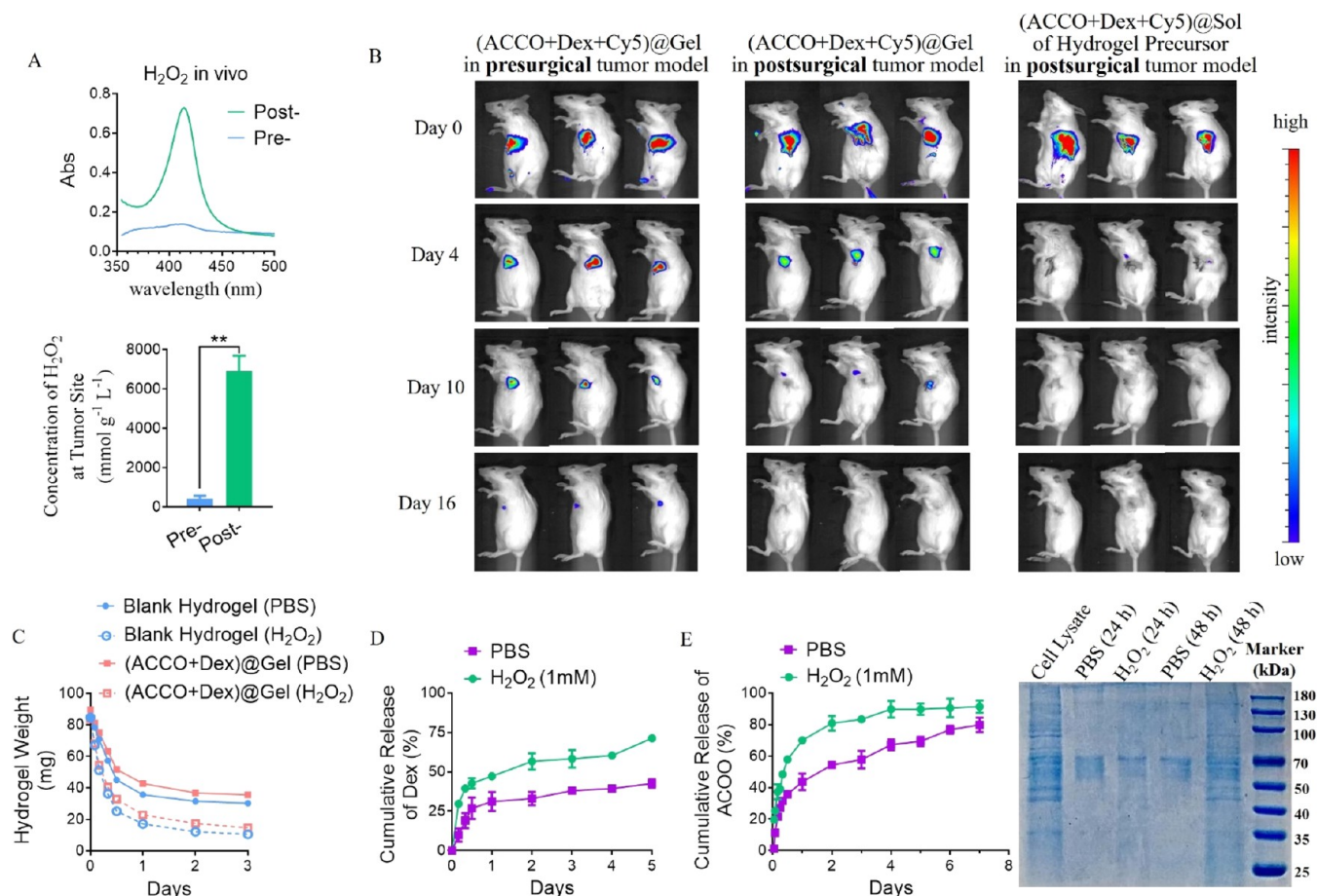


**Figure 4.**  $(ACCO+Dex)@Gel$  responds to enriched ROS in post-surgical trauma. (A) Changes of ROS level in the surgical bed after tumor resection ( $n = 3$ ),  $**p < 0.01$  by Student's  $t$  test. (B) *In vivo* degradation of  $(ACCO+Dex+Cy5)@Gel$  in pre-surgical and post-surgical tumor models ( $n = 3$ ). (C) Degradation of  $(ACCO+Dex)@Gel$ , (D) cumulative release profiles of Dex, and (E) SDS-PAGE electrophoresis of released ACCO from  $(ACCO+Dex)@Gel$  incubated with PBS with or without  $H_2O_2$  (1 mM).

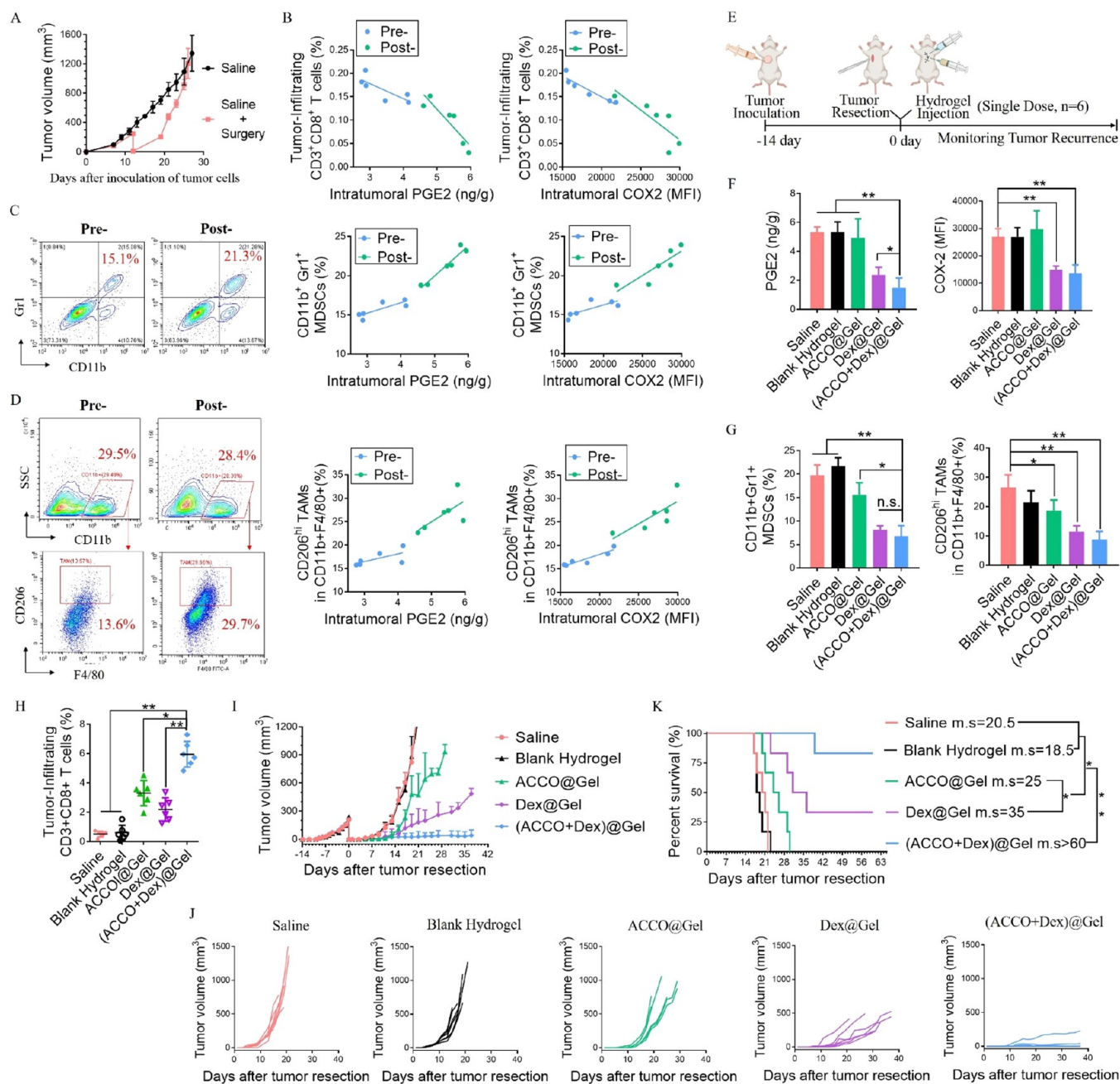
feedback to surgical trauma-induced inflammation.<sup>3</sup> Indeed, Cy5-loaded  $(ACCO+Dex)@Gel$  displaced in the tumor resection cavity degraded relatively faster than the one that was peritumorally injected in a pre-surgical tumor mouse model. Meanwhile,  $(ACCO+Dex+Cy5)@Gel$  retained much longer than hydrogel precursor solution in the resection cavity of post-surgical tumor mouse model (Figure 4B).

In addition, either blank hydrogel or  $(ACCO+Dex)@Gel$  gradually degraded in phosphate buffered saline (PBS, pH 7.4), and their degradation accelerated when immersed in PBS containing 1.0 mM  $H_2O_2$  mimicking the elevated level of ROS in surgical trauma (Figure 4C). Consistently, Dex encapsulated in  $(ACCO+Dex)@Gel$  exhibited higher but not burst release rate in the presence of  $H_2O_2$  (Figure 4D). In a similar trend, the cumulative release of ACCO from hydrogel reached approximately 50% in PBS and over 80% in  $H_2O_2$  containing PBS at 48 h, suggesting that the payload release could be facilitated in a ROS-rich environment. Of note, SDS-polyacrylamide gel electrophoresis analysis further confirmed continuous and controllable release of ACCO. Moreover, as compared with cell lysate, consistent protein shift bands were observed in the released contents from  $(ACCO+Dex)@Gel$  incubated in  $H_2O_2$  for 48 h (Figure 4E). This meant the majority of cellular protein was retained after release. The release of payloads from the hydrogel scaffold into the residual tumors was further investigated *in vivo* after post-surgical

mouse models were locally injected with  $(ACCO+Cy5)@Gel$  at the tumor resection site. Confocal imaging of tumor section (Figure S8) showed substantial fluorescence from both ACCO (pre-stained with CellTracker probe) and Cy5 (fluorescent surrogate for Dex due to similar molecular weight and hydrophobicity) for at least 4 days after the treatment with hydrogel scaffold of  $(ACCO+Cy5)@Gel$ , whereas the treatment with the suspension of ACCO and Cy5 gave rise to a less strong signal that could only be observed for 1 day. The distinct release patterns suggested that the hydrogel scaffold could enable simultaneous and extended delivery of ACCO and Dex into the residual tumor after surgery for immediate, sustainable, and combinatory effects. Collectively, these data showed that the localized platform of  $(ACCO+Dex)@Gel$  could gradually degrade in response to enriched ROS in surgical trauma, which allowed for sustained payload exposure without burst elimination.

#### Reconstruction and Eradication of Residual Tumor.

Before post-surgical intervention, we first analyzed the changes in the tumor microenvironment after surgery. A post-operative breast cancer model was established by resecting approximately 95% of the orthotopic tumors ( $\approx 250\ mm^3$ ) growing in the mammary fat pad of female BALB/c mice. We found that the volume of residual tumor after incomplete resection eventually "caught up" with that of the control tumors (Figure 5A), suggesting that surgical stress rendered remaining tumors



more aggressive. To understand the underlying mechanism, recurrent tumor that regrew to nearly 250 mm<sup>3</sup> were resected, analyzed, and compared with primarily resected tumors (pre-surgical tumors with similar volumes). Immunology analysis confirmed previous findings that immunosuppressive state was consolidated in post-surgical tumors,<sup>10</sup> as evidenced by the less infiltration of CD8<sup>+</sup> T cells (Figure 5B) and higher frequencies of myeloid-derived suppressor cells (MDSCs) (Figure 5C) and tumor-associated macrophages (TAMs) (Figure 5D) in post-

surgical tumors than pre-surgical tumors, and we further revealed that the intratumoral levels of inflammatory cytokines prostaglandin E2 (PGE2) and cyclooxygenase-2 (COX2) were drastically increased after surgery, which negatively correlated with the tumor-infiltrating CD8<sup>+</sup> T cells (Figure 5B) and positively correlated with the abundance of immunosuppressive cells including MDSCs (Figure 5C) and TAMs (Figure 5D). These results provided a solid demonstration that inflammation exacerbated by surgical stress consolidates



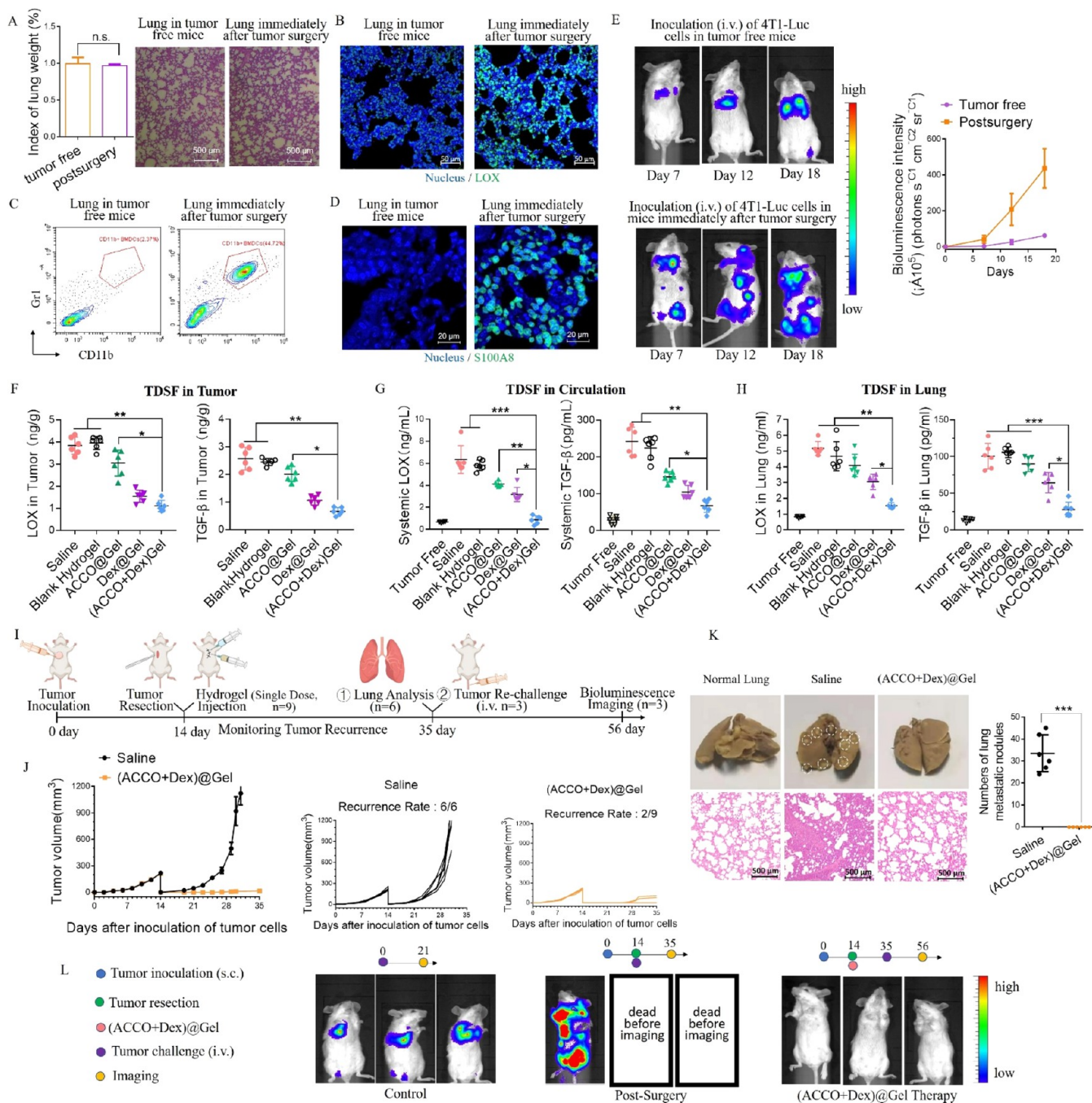


**Figure 6.** (ACCO+Dex)@Gel halts the residual tumor crosstalk with pre-existing PMN and suppresses metastasis. (A) Index of lung weight and hematoxylin–eosin staining histology analysis of lung, (B) immunofluorescence images of pulmonary LOX (green), (C) flow cytometry analysis of pulmonary BMDCs, (D) immunofluorescence images of pulmonary S100A8 (green), and (E) representative bioluminescent images and average bioluminescence intensity of 4T1-Luc progression in tumor-free mice and tumor-resected mice ( $n = 3$ ). (F) Intratumoral, (G) systemic, and (H) pulmonary levels of typical TDSFs (*i.e.*, LOX and TGF- $\beta$ ) 10 days after tumor surgery and local treatments ( $n = 6$ ). Statistical analysis was performed using one-way ANOVA; \* $p < 0.05$ , \*\* $p < 0.01$ , \*\*\* $p < 0.001$ . (I) Schedule for post-surgical intervention, metastasis analysis, tumor rechallenge, and bioluminescence imaging. (J) Overall and individual growth of tumor in post-surgical tumor models treated with (ACCO+Dex)@Gel ( $n = 9$ ). (K) Hematoxylin–eosin histology analysis of pulmonary metastatic nodule ( $n = 6$ ). \*\*\* $P < 0.001$  by Student's  $t$  test. (L) Representative bioluminescent images of post-surgical tumor models that consecutively received local treatment with (ACCO+Dex)@Gel and intravenous rechallenge of 4T1-Luc breast cancer cells ( $n = 3$ ).

immunosuppression in residual tumor microenvironment, highlighting the great essentiality to alleviate inflammation at tumor resection for potentiating ACCO-based therapy.

We then investigated the effect of (ACCO+Dex)@Gel on shaping and inhibiting residual tumors after surgery. An orthotopic breast tumor recurrence model after an incomplete

tumor resection was established. Surgery was conducted in 4T1 tumor-bearing mice with approximately 5% tumor tissue left intentionally. Immediately afterward, one single dose of various hydrogel formulations was injected into the tumor resection cavity, and tumor recurrence was monitored (Figure 5E). Immunology analysis of residual tumor was conducted on

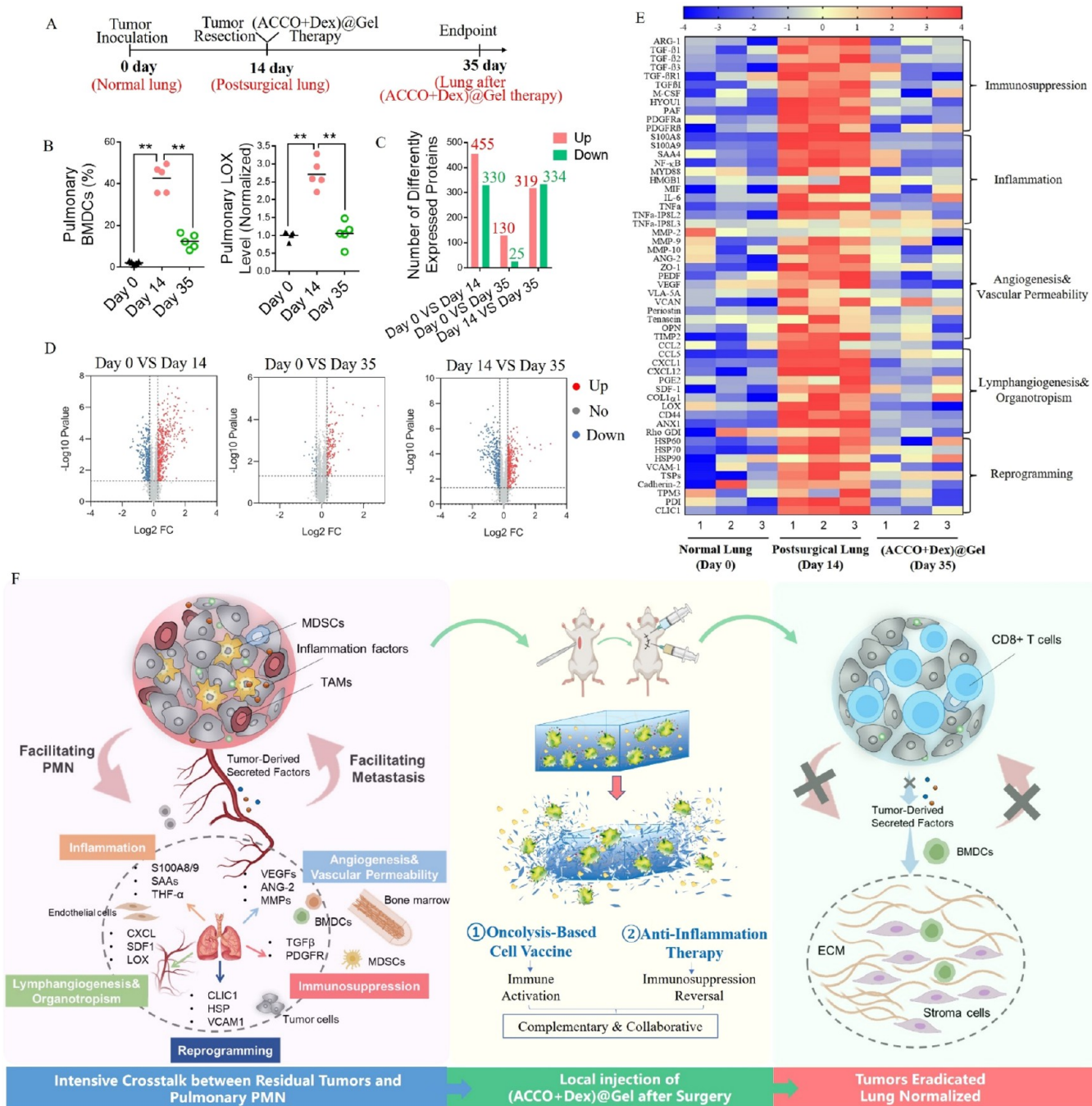


**Figure 7.** (ACCO+Dex)@Gel regresses pulmonary PMN and normalizes lung. (A) Schematic schedule for *ex vivo* analysis of lungs at different stages. (B) Analysis of BMDCs and LOX accumulation in lungs at different stages. (C) Numbers of differently expressed proteins and (D) volcano plot analysis of pulmonary proteins at different stages ( $n = 3$ ). (E) Heat map for protein expressions associated with the key characteristics of pulmonary PMN formation before and after (ACCO+Dex)@Gel treatment. (F) Mechanistic illustration of (ACCO+Dex)@Gel to exert local effect on ameliorating immune microenvironment and abscopal effect on normalizing pre-metastatic sites. Statistical analysis was performed using one-way ANOVA; \* $p < 0.05$ , \*\* $p < 0.01$ .

Day 10 after local treatments. As expected, surgery left an intractable environment in residual tumors of saline or blank hydrogel treated mice, with overexpression of inflammatory PGE2, COX-2 (Figure 5F) and related cytokines (e.g., IL-4, IL-10, TNF- $\alpha$ , Figure S9), abundant residence of immunosuppressive MDSMs and TAMs (Figure 5G), and poor infiltration of antitumor CD8+ effector cells (Figure 5H). Consequently, post-surgical mice treated with saline or blank hydrogel experienced a rapid tumor regrowth (Figure 5I,J). Although

ACCO@Gel recruited some tumor-infiltrating CD8+ T cells, ACCO@Gel alone had moderate impact on reducing the inflammation, which maintained MDSMs and TAM at a high level to dampen tumor antigens presentation and impair T cell function. In contrast, Dex@Gel effectively primed the landscape of residual tumors by alleviating the inflammation, attenuating the quantity of inflammation-oriented MDSMs, and repolarizing TAMs toward M1 phenotype (Figure 5G and Figure S10), which may unleash the pre-existing T cells,<sup>36</sup> but



Dex@Gel failed to mobilize T cell to tumors due to a lack of tumor immunogenicity. These results explained the observation that the monotherapy of ACCO@Gel or Dex@Gel only resulted in partial inhibition of residual tumors with 100% recurrent rate after surgery. Notably, (ACCO+Dex)@Gel coordinated the complementary functions of (1) immunostimulatory ACCO-induced immunization and (2) anti-inflammatory Dex-dominated immunosuppression reversal, which contributed to considerable inhibition of residual tumors after surgery, even showing complete eradication in 66.7% mice. As the result of excellent therapeutic outcome, (ACCO+Dex)@Gel substantially extended the mice survival as compared with other controls (Figure 5K).

**Interception of Seed–Soil Crosstalk and Post-Surgical Suppression of Metastasis.** As evidenced by no change in the index of lung weight or histology of lung lobe sections, early metastasis was not detected by the time the surgical resection of primary tumor was performed (Figure 6A). However, we did observe key characteristics and major components crucial for the pulmonary formation of a pre-metastatic niche (PMN). Substantial accumulation of tumor-derived secreted factor (TDSF) lysyl oxidase (LOX, Figure 6B), recruitment of tumor-mobilized bone marrow-derived cells (BMDCs, Figure 6C), and secretion of metastasis-promoting factor S100A8 (Figure 6D) were found in the lung of mice that immediately received tumor surgery, indicating PMN establishment before surgery. This complied with the seed and soil hypothesis that, ahead of metastasis, primary tumors can prepare fertile soil in distant organs for colonization of metastatic tumor cell seeds. For instance, one of the key mechanisms to initiate PMN is that the primary tumor releases LOX that eventually accumulates at future metastatic sites in distant organ and recruits BMDCs, which thereafter produces various factors including S100A8 to create PMN where the microenvironment is hospitable for metastasis.<sup>5,37</sup> Indeed, we have also revealed that, although the primary tumor was mostly removed, the impact of pre-existing PMN on promoting metastasis were not abrogated in post-surgical model. As shown in Figure 6E, despite the fact that a primary tumor was absent in both mice models, as compared with the tumor-free mice without the impact of PMN, the metastasis of disseminating 4T1 cells was drastically facilitated in a post-surgical tumor mice model. Similar phenomena have also been seen in the same or other post-surgical tumor models.<sup>38,39</sup> Collectively, these results suggested that post-surgical intervention was required to not only eradicate residual tumors but also resist the impact of established PMN in distant organs to promote metastasis of recurrent tumor seeds.

Because inflammation or hypoxia is known to induce tumor cells to produce more TDSFs that are subsequently released into blood and enter a distant site to maintain and facilitate PMN,<sup>5</sup> we then investigated the impact of locally administered (ACCO+Dex)@Gel on this seed–soil crosstalk by measuring the intratumoral (Figure 6F), systemic (Figure 6G), and pulmonary (Figure 6H) levels of typical TDSFs (*i.e.*, LOX and TGF- $\beta$ ). As compared with saline and blank hydrogel groups that had high levels of TDSFs in tumor, blood, and lung, ACCO@Gel only moderately reduced TDSFs. Due to the ability to alleviate inflammation, Dex@Gel showed significantly better effect than ACCO@Gel on decreasing the TDSFs production in tumor, release in circulation, and accumulation in lung. In addition, (ACCO+Dex)@Gel resulted in a further

reduction of TDSFs in residual tumors, and even showed similar levels of systemic and pulmonary TDSFs when compared with that of tumor-free normal mice (Figure 6F–H). This may be explained by two mechanisms: (1) inflammation alleviation inhibited the generation and secretion of TDSFs by tumor cells and (2) inflammation alleviation resuscitated ACCO that elicited antitumor immunity to reduce the number of tumor cells producing TDSFs, together contributing to the interception of seed–soil crosstalk.

Meanwhile, in another individual experiment (Figure 6I), (ACCO+Dex)@Gel had reproducible efficacy to considerably inhibit residual tumors after surgery, with significant drop of recurrence rate to ~22% (Figure 6J). Furthermore, the post-surgical treatment with (ACCO+Dex)@Gel completely prevented the occurrence of pulmonary metastasis, whereas the saline group experienced a high burden of metastatic nodules in the lung (Figure 6K). Afterward, a tumor rechallenge experiment was performed on the cured mice (Figure 6L). In the control group, a rechallenge of intravenously injected 4T1 cells caused systemic metastasis and high mortality in mice that only received surgery, with a degree much more severe than in tumor-free mice, providing additional evidence that the effect of PMN still exists even after the tumor was resected. Strikingly, orthotopic 4T1 tumor bearing mice cured from sequential tumor resection and post-surgical intervention with (ACCO+Dex)@Gel were completely resistant to a secondary challenge of disseminating 4T1 cells. Such a promising effect could be partially ascribed to the activation of antigen-specific antitumor immunity systemically and partially ascribed to the abrogation of pro-metastatic seed–soil mechanisms, which needs further validation.

**Regression of Pre-Existing PMN.** It is well-documented that metastasis is initiated by two indispensable factors of residual tumor seeds and distant PMN soil.<sup>5</sup> Having demonstrated the local effect of (ACCO+Dex)@Gel on the eradication of residual tumor seeds and interception of seed–soil crosstalk, we next sought to investigate its abscopal effect on modulating PMN soil in distant lung. To this end, we analyzed the lungs at different stages shown in Figure 7A, which included the normal lung (Day 0), post-surgical lung (Day 14), and repaired lung after (ACCO+Dex)@Gel treatment (Day 35). As compared with the normal lung without PMN, post-surgical lung had a higher accumulation of BMDCs and LOX, which fostered the PMN formation. Meanwhile, subsequent treatment with (ACCO+Dex)@Gel significantly decreased pulmonary BMDCs and LOX, indicating the regression of PMN (Figure 7B). Further proteomics study revealed a large number of proteins expressed differently between a normal lung and post-surgical lung, probably due to the PMN progression; post-surgical intervention with (ACCO+Dex)@Gel drastically narrowed the difference between the normal lung and repaired lung, while changing the landscape between the post-surgical lung and repaired lung (Figure 7C,D). As PMN could be defined by six characteristics including immunosuppression, inflammation, angiogenesis/vascular permeability, lymphangiogenesis, organotropism, and reprogramming,<sup>5</sup> we further looked into a diversity of relevant signal and molecular pathways. As shown in Figure 7E and Table S1, a majority of PMN-associated factors were upregulated in post-surgical lung compared with those in a normal lung. Sequential treatment with (ACCO+Dex)@Gel after surgery could reverse the PMN progression and normalize the lung to a state similar to a PMN-free lung.

Thus, local implantation of (ACCO+Dex)@Gel at tumor surgical cavity exerted abscopal effect on disrupting pulmonary PMN as well, further reducing the risk of metastasis.

Theoretically, residual tumors after incomplete resection are more prone to recur and metastasize, due to the intensive crosstalk between local tumor microenvironment and distant metastatic sites: inflammation and immunosuppression induced by surgical stress awaken dormant cancer cell seeds and stimulate them to produce various TDSFs, which influences mobilization and recruitment of BMDCs into the secondary sites, altering and fertilizing the microenvironment to create PMN; in return, PMN secretes chemokines to attract tumor cells and provides favorable soil to support their seeding, colonization, outgrowth, and expansion, resulting in metastasis.<sup>5</sup> It was exciting to see that local injection with (ACCO+Dex)@Gel at tumor resection site enabled sustainable release of immunoadjuvant ACCO and anti-inflammatory Dex, which work jointly to shape the immune landscape in post-surgical environment, leading to the eradication of residual tumor. As a result, seed–soil crosstalk was intercepted. Without the maintenance and facilitation of a primary tumor, and probably with the systemic elicitation of antitumor immunity, PMN was regressed and the pre-metastatic sites in distant organ were normalized (Figure 7F).

In the present study, we utilized immunocompetent inbred female mice of BALB/c strains to generate a syngeneic model of 4T1 murine breast cancer orthotopically growing in the mammary fat pad and surgically resected the tumors to faithfully recapitulate the post-operative breast cancer metastasis and evaluate the combinatory effect of inflammation alleviation and ACCO immunization. This orthotopic model closely mimics the human-like evolution of spontaneous breast cancer metastasis after surgery and supports the presence of immune effector.<sup>40,41</sup> Of note, differences between murine and human immune systems do exist, which may directly impact the immunotherapy evaluation.<sup>42</sup> Recently, successful attempts have been made to humanize mouse models that resemble immune systems in humans.<sup>43</sup> To gain information that more precisely reflects the clinical relevance, future work will apply the strategy on humanized mice.

## CONCLUSION

In this study, we have designed a trauma-responsive scaffold that was formed *in situ* and gradually released immunoadjuvant ACCO and anti-inflammatory Dex for post-operative suppression of cancer metastasis. The work has dealt with the longstanding challenges for the application of cancer vaccine after surgery, including (i) poor immunogenicity and tumor heterogeneity, (ii) immunosuppressive and pro-metastatic microenvironment, and (iii) insufficient immune stimulation. First, self-adjuncting ACCO, with a whole array of tumor antigens and surface exposure of oncolysis-orchestrated DAMPs, was developed as a highly immunogenic cell vaccine to recruit immune effector against autologous microtumor residuals. Since it was not necessary to induce onsite oncolysis in scattering tumor cells at resection trauma where targeted delivery was difficult and antigen sources were insufficient, ACCO in the form of a cell vaccine further extended the application of oncolytic therapy in post-surgical intervention. Second, we demonstrated that concurrent inflammation alleviation reversed the local immunosuppression at surgical site to resuscitate ACCO and further intercepted the seed–soil crosstalk to attenuate the metastasis-promoting impact from

pre-existing PMN at distant lung. Third, we coordinated an ACCO vaccine and anti-inflammatory therapy within one hydrogel scaffold that responded to enriched ROS in trauma for post-surgical drug delivery, spatiotemporal payload release, microenvironment reconstruction, and sustained immune stimulation. Notably, a single dose of (ACCO+Dex)@Gel exerted a local effect on priming immune landscape while eradicating residual tumors and abscopal effect on regressing pulmonary PMN, thus achieving a two-pronged strategy for the simultaneous elimination of asynchronous seeds and soil at different regions to inhibit metastasis after surgery.

## EXPERIMENTAL SECTION

**Cell Lines and Animals.** 4T1 murine breast tumor cell, luciferase-expressing 4T1 cells (4T1-Luc), and B16 murine melanoma cells were purchased from Chinese Academy of Science Cell bank (Shanghai, China), cultured in RPMI-1640 medium (Gibco) supplemented with 10% v/v fetal bovine serum (FBS), 100 U/mL penicillin, and 100  $\mu$ g/mL streptomycin, and incubated in a 37 °C humidified environment with 5% CO<sub>2</sub> supply. BALB/c female mice (6–8 week, 18–22 g, SPF) were purchased from Dashuo Experimental Animal Company (Chengdu, China). All of the animal experiments were approved by the Medical Ethics Committee of Sichuan University, and the animal experiments were performed in the Animal Laboratory of West China School of Pharmacy in Sichuan University (accreditation number: SYXK(Chuan)2018-113).

**Preparation and Characterization of ACCO.** 4T1 cell suspension was incubated with 50  $\mu$ M oncolytic peptide LTX-315 (amino acid sequence: CKKWWKKW(Dip)K-NH<sub>2</sub>, Shanghai Apeptide Co., Ltd., Shanghai, China) at 37 °C for 4 h. Then, the suspension was centrifuged (3000 rpm for 5 min), the cell pellet was washed with PBS, and ACCO was collected as the final product.

To demonstrate oncolysis, membrane disruption within ACCO was investigated. To visualize membrane lysis on the cell surface, ACCO was fixed by 4% paraformaldehyde and 2.5% glutaraldehyde in PBS for 15 min at 25 °C. Fixed cells were dehydrated in a graded series of ethanol (30%, 50%, 70%, 90%, and 100%), dried by a critical point dryer, and surface coated with gold prior to examination with SEM (FEI Quanta 600 FEG). To investigate the lysosome rupture and cell membrane permeability, ACCO was consecutively incubated with LysoTracker Green for 30 min and propidium iodide for 10 min at 37 °C, respectively, prior to analysis by flow cytometry. To investigate the mitochondrial membrane potential, ACCO was stained with JC-1 (5,5',6,6'-tetrachloro-1,1',3,3'-tetraethylbenzimidazolylcarbocyanine iodide, MedChemExpress) for 30 min, washed with PBS, and analyzed by flow cytometry (FACSCelesta, BD) using 488 nm excitation with 530/30 and 585/42 nm band-pass filters.

To demonstrate the immunogenicity of ACCO, we analyzed the induction of DAMPs including CRT exposure, ATP secretion, and HMGB1 release after incubation of ACCO in fresh culture medium for 24 h. For CRT measurement, ACCO was pre-blocked with 5% goat serum, incubated with CRT primary antibody (1:500, abcam, ab2907) at 4 °C for 1 h, washed with PBS, further incubated with secondary Alexa Fluor 647-conjugated antibody (1:1000, ab150077) at 4 °C for 30 min, and washed again prior to analysis by flow cytometry (Beckman Coulter, California). For quantification of extracellular ATP, the supernatant of ACCO suspension was collected for ATP concentration detection by an ATP Assay Kit (Beyotime S0026). In addition, HMGB1 released in the supernatant was measured by Western blot according to the protocol as previously reported. Then, relevant mechanism studies were conducted. Intracellular ROS production was measured by treating ACCO with 10  $\mu$ M 2',7'-dichlorodihydrofluorescein diacetate (DCFH-DA) for 20 min at 37 °C, followed by cell wash and fluorescence intensity measurement of activated DCF-DA by flow cytometry, according to the instructions of a Reactive Oxygen Species Assay Kit (Beyotime). ER stress induction was investigated by fixing and permeabilizing ACCO with transcription factor buffer set (BD Biosciences) as



manufacturers' instructions, followed by incubating with anti-CHOP polyclonal antibody (1:500 dilution, Abcam) in 1% bovine serum albumin (BSA) for 1 h at 4 °C, further staining with Alexa Fluor 647 labeled IgG (H+L) secondary antibody (1:1000 dilution, Abcam) for 40 min at 4 °C, and analysis by flow cytometry. 4T1 cells that were pre-incubated with GSH (20 mM, 2 h) and then coincubated with LTX-315 peptide (50  $\mu$ M, 4 h) were set as a control. To investigate the phagocytosis of ACCO, bone marrow-derived macrophages (BMDMs) were isolated and cultured according to the protocol as previously reported.<sup>44</sup> Then, ACCO and BMDMs were labeled with cell membrane labeling tracer DiO (3,3'-diocadecyloxycarbocyanine perchlorate, Meilunbio) and DiI (1,1'-diocadecyl-3,3,3',3'-tetramethylindocarbocyanine perchlorate, Meilunbio), respectively. Afterward, DiO-labeled ACCO and DiI-labeled BMDMs were mixed at a 1:1 ratio and incubated at 37 °C for 4 h, prior to confocal microscope imaging and flow cytometry analysis. For the above experiments, 4T1 cells that were treated with chemodrug Dox (10  $\mu$ M, 24 h) were set as a control.

**Preparation and Characterization of (ACCO+Dex)@Gel.** ROS-labile  $N^1$ -(4-boronobenzyl)- $N^3$ -(4-boronophenyl)- $N^1,N^1,N^3,N^3$ -tetramethylpropane-1,3-diaminium (TSPBA), as the hydrogel cross-linker, was synthesized as previously described<sup>31</sup> and further confirmed by <sup>1</sup>H NMR and mass spectrometry showing a major peak at  $m/z$  200.12 from the molecular ion peak ( $C_{21}H_{34}B_2N_2O_4^{2+}$ ,  $M_w = 200.12$ ) of TSPBA ( $C_{21}H_{34}B_2Br_2N_2O_4$ ,  $M_w = 559.94$ ). For the preparation of (ACCO+Dex)@Gel, ACCO ( $1 \times 10^6$  cells) were suspended in 100  $\mu$ L (5 wt %) of hydrogel precursor poly(vinyl alcohol) (PVA;  $\sim 75$  kDa; 99% hydrolyzed; Aladdin Biotech Co., Ltd.). Dexamethasone (Dex, Shanghai yuanye Bio-Technology Co., Ltd., Shanghai, China) with a concentration of 12.5 mM in 40  $\mu$ L of PEG-400 solution was mixed with 60  $\mu$ L of TSPBA (83.3 wt %) solution to form the cross-linker solution. (ACCO+Dex)@Gel was immediately formed when mixing the cross-linker solution with an equivalent volume of PVA solution. Therefore, the concentrations of ACCO and Dex within the hydrogel scaffold ( $\sim 200$   $\mu$ L) were calculated to be  $1 \times 10^6$  cells/200  $\mu$ L and 0.2 mg/200  $\mu$ L, respectively.

The morphology of PVA solution, blank hydrogel, or (ACCO+Dex)@Gel was characterized by a scanning electron microscope (SEM, SU3500/Aztec X-Max20). The dynamic rheological behavior of PVA and hydrogel was measured at 25 °C using a TA Instruments AR 2000 rheometer with a shear strain of 1% and oscillation frequency from 0.1 to 10 rad/s. The mechanical and adhesive properties of the hydrogel were measured at 25 °C using a TA Instruments AR 2000 rheometer. To investigate the distribution of ACCO in hydrogel, CRT, cytoplasm, and nucleus of ACCO were stained with anti-CRT primary antibody/secondary Alexa Fluor 647-conjugated antibody, CellTracker Green 5-chloromethylfluorescein diacetate (CMFDA), and Hoechst 33342, respectively, and further loaded in the hydrogel. Afterward, a three-dimensional construction image was analyzed using a confocal microscope (CLSM, Zeiss LSM 510 DUE, Jena, Germany).

To investigate the degradation and payload release, (ACCO+Dex)@Gel was immersed into PBS (pH 7.4) with or without H<sub>2</sub>O<sub>2</sub> (1 mM) at 37 °C. At each designated time intervals, the weight of the hydrogel was recorded. Meanwhile, payload released in buffer was detected. The Dex concentration in the collected solutions was analyzed by high-performance liquid chromatography. ACCO released in the collected solutions was lysed, centrifuged, mixed with gel loading buffer, boiled at 100 °C for 10 min, and then electrophoresed on 8% SDS-PAGE. Then, the full-size image was captured. All experiments were performed in triplicate.

To investigate the degradation *in vivo*, the H<sub>2</sub>O<sub>2</sub> level in the surgical sites was first measured *via* a hydrogen peroxide assay kit (Jiancheng Bioengineering Institute). Then, cyanine 5 (Cy5, 4 nmol, Meilunbio, Dalian, China) was loaded in (ACCO+Dex)@Gel or mixed with hydrogel precursor suspension containing ACCO and Dex. Afterward, 200  $\mu$ L of Cy5-labeled formulation was subcutaneously injected in a surgical bed of post-surgical mouse model after resection of orthotopic 4T1 breast tumors (250 mm<sup>3</sup>) or the same

region of a pre-surgical mouse model. Fluorescence imaging was recorded on day 0, 4, 10, and 16 using an IVIS Spectrum *In Vivo* Imaging System (PerkinElmer, Lumina 3). To investigate the release of payloads from the hydrogel, ACCO was pre-labeled with CMFDA, and Cy5 was selected as the fluorescent surrogate for Dex. Then, mice after tumor incomplete resection were locally injected with either suspension of ACCO+Cy5 or (ACCO+Cy5)@Gel. On day 1, 2, and 4 post treatment, residual tumor tissues were collected, cryo-sectioned, and analyzed using confocal microscopy imaging.

**Vaccination Assay.** Healthy female BALB/c mice ( $n = 6$ ) were vaccinated twice by subcutaneous injection with 100  $\mu$ L of ACCO@Gel at the right flank. Then, 4T1 cells ( $5 \times 10^5$ ) were orthotopically injected into the third mammary fat pad of mice. Tumor size and body weight were recorded every other day, and tumor size was calculated as follows: tumor volume (mm<sup>3</sup>) =  $1/2 \times \text{width}^2 \times \text{length}$ . ACCO suspension without gelation, nI-ACC@Gel derived from boiled 4T1 cells, nA-CCO@Gel derived from LTX-315 oncolytic peptide-treated B16 cells, and ACC-Dox@Gel derived from Dox-treated 4T1 cells were prepared with a similar procedure as described above and used as a control.

**Immune Status Investigation after Vaccination Assay.** At the end point of vaccination assay (20 days after tumor cell inoculation), vaccinated mice in various groups ( $n = 6$ ) were sacrificed, and recurrent tumors were collected, cut into small pieces, and dissociated in digestion buffer. Then, single cell suspension from tumor tissue was obtained by filtering the buffer through a 70  $\mu$ m nylon strainer, lysing red blood cells by incubating with ACK lysing buffer (4 °C, 10 min, Thermo Scientific), washing cells twice with cold PBS, and suspending cells in PBS. For analysis of tumor-reactive CD8<sup>+</sup> T cells (CD3<sup>+</sup>CD4<sup>-</sup>CD8<sup>+</sup>IFN- $\gamma$ <sup>+</sup>) and activated tumor-infiltrating DCs (CD80<sup>+</sup>CD86<sup>+</sup>CD11c<sup>+</sup>), tumor cell suspensions were fixed with 4% paraformaldehyde, incubated with anti-CD16/32 antibody to block nonspecific interaction with Fc receptors (4 °C, 30 min), and then stained with anti-CD3-FITC (1:200 dilution), anti-CD8-APC (1:300 dilution), anti-CD4-PerCP (1:150 dilution), anti-IFN- $\gamma$ -PE (1:200 dilution), anti-CD11c-FITC (1:300 dilution), anti-CD80-PE (1:300 dilution), or anti-CD86-APC (1:300 dilution) at 4 °C for 60 min, according to the instructions of the manufacturer. Afterward, cells were washed and analyzed by flow cytometry. To investigate the establishment of durable immunity, single-cell suspensions isolated from spleens were fixed, pre-blocked, and stained with anti-CD62L-PerCP-Cy5.5, anti-CD44-PE, and anti-CD8-APC antibodies to identify effector memory T cells (CD62L<sup>-</sup>CD44<sup>+</sup>CD8<sup>+</sup>) by flow cytometry. To measure the intratumoral PD-L1 expression, tumor cell suspensions were blocked with anti-CD16/32 antibody and stained with anti-CD45-PC5.5 and anti-PD-L1-APC antibodies as described above.

**Therapeutic Efficacy Investigation of ACCO@Gel Vaccination Combining with Anti-PD-L1 Therapy.** Healthy female BALB/c mice ( $n = 6$ ) were vaccinated twice by subcutaneous injection with 100  $\mu$ L of ACCO@Gel at the right flank at 30 days and 15 days before orthotopic injection of 4T1-Luc cells ( $5 \times 10^5$ ) into the mammary fat pad of mice. Three doses of antimouse  $\alpha$ -PD-L1 antibody (100  $\mu$ g per mouse; Clone: 10F.9G2; BioXcell) were intraperitoneally administered at day 7, 9, and 11 after tumor cell inoculation. Bioluminescence images were used to monitor the progression of 4T1-Luc tumors and captured on the day 0, 8, and 14 with an IVIS Spectrum Imaging System (PerkinElmer Ltd.). Living Image software (PerkinElmer Ltd.) was used to acquire the data 10 min after intraperitoneal injection of D-luciferin (Dalian Meilun Biotech Co., Ltd., Dalian, China, 15 mg kg<sup>-1</sup>) into the animals.

**Investigation of Post-Surgical Alteration in Residual Tumor Microenvironment.** To establish post-operative breast cancer model, surgery was performed on female BALB/c mice (6–8 weeks) orthotopically bearing 4T1 tumors ( $\sim 250$  mm<sup>3</sup>) on day 14 after 4T1 ( $1 \times 10^6$ ) cells were injected into the mammary fat pad of mice. Approximately 95% of the tumors were resected with 5% tumor tissue left intentionally. The resected tumors were collected as pre-operative tumors. When the volume of residual tumors regrew to nearly 250 mm<sup>3</sup> on day 20, tumors were collected as post-operative

tumors ( $n = 6$ ). For flow cytometry analysis of immune cells, single cell suspension from pre-operative and post-operative tumors were isolated, collected, fixed, pre-blocked, and stained with antibodies against as described above. To identify MDSCs (CD11b+Gr1+), cell suspensions were stained with anti-Gr1-FITC (1:300 dilution) and anti-CD11b-PE (1:300 dilution) at 4 °C for 1 h. To identify TAMs (CD11b+F4/80+CD206hi), cell suspensions were stained with anti-CD11b-PE (1:300 dilution), anti-F4/80-FITC (1:300 dilution), and anti-CD206-APC (1:300 dilution) at 4 °C for 1 h. To investigate the COX-2 expression in tumor, cells were permeabilized by transcription factor buffer set as manufacturer's instructions and stained with anti-COX-2 primary antibody (1:500) at 4 °C for 1 h, followed by incubation with secondary Alexa Fluor 647-conjugated antibody (1:1000) at 4 °C for 40 min. The intratumoral concentration of PGE2 in cell suspension before ACK lysing was measured using a mouse PGE2 ELISA kit (Shanghai Enzyme-linked Biotechnology) after centrifugation and collecting the supernatant.

**Evaluation of the Formation of Pulmonary PMN after Surgical Removal of the Primary Tumor.** Lungs collected from tumor-free normal BALB/c mice and post-surgical BALB/c mice immediately undergoing resection of orthotopic 4T1 tumor (~250 mm<sup>3</sup>) were analyzed and compared ( $n = 3$ ). Lung metastasis was assessed by the index of lung weight to body weight and hematoxylin–eosin staining histology analysis. To evaluate pulmonary recruitment of CD11b+ BMDCs, cell suspension from lungs were prepared as described above and stained with anti-CD11b-PE (1:300) and anti-Gr1-FITC (1:300), followed by flow cytometry. Pulmonary accumulation of LOX and S100A8 were detected by immunofluorescence staining of frozen lung section (10 μm) with primary anti-LOX antibody or anti-S100A8 antibody and fluorescence-labeled secondary antibodies, followed by confocal laser scanning microscopy imaging.

To investigate the impact of PMN formation on metastasis, 4T1-Luc cells ( $1 \times 10^6$ ) were intravenously injected in tumor-free normal mice and post-surgical mice immediately undergoing resection of primary 4T1 tumors. Bioluminescence images were used to monitor the metastasis of 4T1-Luc tumors. Prior to IVIS spectrum imaging, mice were intraperitoneally injected with D-luciferin potassium salt (15 mg/mL, 200 μL).

**Post-Operative Inhibition of Tumor Recurrence.** Post-operative breast cancer model with a recurrent tumor was established as described above. Immediately after surgery, mice were randomly divided into five groups ( $n = 6$ ) and locally injected with a single dose (~200 μL) of *in situ* forming blank hydrogel, Dex@Gel, ACCO@Gel, and (ACCO+Dex)@Gel at the resection cavities. The equivalent doses for Dex and ACCO were 10 mg/kg and  $1 \times 10^6$  cells/mouse, respectively. Tumor size and animal survival were recorded every other day until 40 days post operation. In another individual experiment, mice were sacrificed on day 10 after local treatments, and tumor tissues were collected for the analysis of alterations in immune status of residual tumor microenvironment. Frequencies of CD3<sup>+</sup>CD8<sup>+</sup> immune T cells, CD86<sup>+</sup>CD11b<sup>+</sup>F4/80<sup>+</sup> M1 macrophage, immunosuppressive cells (CD11b<sup>+</sup>Gr1<sup>+</sup> MDSCs and CD206<sup>hi</sup> CD11b<sup>+</sup>F4/80<sup>+</sup> TAMs), and intratumoral level of inflammatory factors (PGE2 and COX-2) were evaluated as described above. For the detection of the levels of TDSFs (TGF-β and LOX) in circulation, peripheral blood, tumor, and lung tissue were collected. Serum obtained by centrifugation of peripheral blood and supernatant of tumor and lung cell suspension were used for a Mouse LOX Elisa kit (Wuhan ColorfulGene Biological Technology Co., Ltd., Wuhan, China) and a Mouse TGF-β Elisa kit (Quanzhou Ruixin Biological Technology Co., Ltd., Quanzhou, China) assaying, respectively.

**Post-Operative Prevention of Tumor Metastasis.** To investigate the therapeutic efficacy of (ACCO+Dex)@Gel on preventing post-operative tumor metastasis, a post-operative breast cancer model with recurrent tumor and spontaneous metastasis was established as described above, treated with (ACCO+Dex)@Gel, and rechallenged with disseminating 4T1 cells. Briefly, 4T1 cells ( $1 \times 10^6$ ) were injected into the mammary fat pad of mice on day 0. Orthotopic grown tumors were resected with ~5% residual tumor left

intentionally on day 14. Immediately after surgery, mice were locally treated with a single dose (~200 μL) of (ACCO+Dex)@Gel *in situ* formed at the resection cavities (Dex, 10 mg/kg; ACCO,  $1 \times 10^6$  cells/mouse). On day 35, mice were either sacrificed for hematoxylin and eosin staining histology analysis of pulmonary metastasis ( $n = 6$ ) or further intravenously rechallenged with 4T1-Luc cells ( $1 \times 10^6$ ). On day 56, bioluminescence images of rechallenged mice were obtained to illustrate the long-term effect on preventing metastasis.

In another individual experiment, lungs were collected on day 0, 14, and 35 from mice receiving post-surgical intervention with (ACCO+Dex)@Gel. PMN-fostering factors including pulmonary accumulation of LOX and recruitment of BMDCs were analyzed and compared as described above. For the analysis of the changes of various PMN-associated protein expression levels in lung, lung and tissue samples were sent for proteomics analysis (Shanghai Omicspace Biotech Co., Ltd., Shanghai, China) including protein extraction, protein digestion, TMT labeling, LC–MS analysis, and mass spectrometry database analysis.

**Statistical analysis.** Statistical significance analysis was performed for all proteins with quantitative data (*t*-test). The proteins with significant difference were screened according to a *P*-Value <0.05. Then, volcano plot and cluster analysis were performed on the selected proteins.

## ASSOCIATED CONTENT

### Supporting Information

The Supporting Information is available free of charge at <https://pubs.acs.org/doi/10.1021/acsnano.1c11562>.

Figures of confocal imaging and flow cytometry analysis, strain sweep dynamic rheological data, compressive and tensile stress–strain curves, tensile adhesion tests and shear adhesion tests, body weight change, histological analysis of different organs, tumor growth curves, semi-quantification of tumor bioluminescence intensities in mice, and *in vivo* release of payloads from the hydrogel scaffold and table of abbreviations for proteomics study (PDF)

## AUTHOR INFORMATION

### Corresponding Authors

**Yuan Huang** – Key Laboratory of Drug-Targeting and Drug Delivery System of the Education Ministry and Sichuan Province, Sichuan Engineering Laboratory for Plant-Sourced Drug and Sichuan Research Center for Drug Precision Industrial Technology, West China School of Pharmacy, Sichuan University, Chengdu 610041, China; [orcid.org/0000-0003-3410-8602](https://orcid.org/0000-0003-3410-8602); Email: [huangyuan0@163.com](mailto:huangyuan0@163.com)

**Lian Li** – Key Laboratory of Drug-Targeting and Drug Delivery System of the Education Ministry and Sichuan Province, Sichuan Engineering Laboratory for Plant-Sourced Drug and Sichuan Research Center for Drug Precision Industrial Technology, West China School of Pharmacy, Sichuan University, Chengdu 610041, China; [orcid.org/0000-0002-3616-8206](https://orcid.org/0000-0002-3616-8206); Email: [liliantriple@163.com](mailto:liliantriple@163.com)

### Authors

**Junlin Li** – Key Laboratory of Drug-Targeting and Drug Delivery System of the Education Ministry and Sichuan Province, Sichuan Engineering Laboratory for Plant-Sourced Drug and Sichuan Research Center for Drug Precision Industrial Technology, West China School of Pharmacy, Sichuan University, Chengdu 610041, China

**Ping Zhang** – Key Laboratory of Drug-Targeting and Drug Delivery System of the Education Ministry and Sichuan Province, Sichuan Engineering Laboratory for Plant-Sourced



Drug and Sichuan Research Center for Drug Precision Industrial Technology, West China School of Pharmacy, Sichuan University, Chengdu 610041, China

**Minglu Zhou** – Key Laboratory of Drug-Targeting and Drug Delivery System of the Education Ministry and Sichuan Province, Sichuan Engineering Laboratory for Plant-Sourced Drug and Sichuan Research Center for Drug Precision Industrial Technology, West China School of Pharmacy, Sichuan University, Chengdu 610041, China

**Chendong Liu** – Key Laboratory of Drug-Targeting and Drug Delivery System of the Education Ministry and Sichuan Province, Sichuan Engineering Laboratory for Plant-Sourced Drug and Sichuan Research Center for Drug Precision Industrial Technology, West China School of Pharmacy, Sichuan University, Chengdu 610041, China

Complete contact information is available at:

<https://pubs.acs.org/10.1021/acsnano.1c11562>

## Notes

The authors declare no competing financial interest.

## ACKNOWLEDGMENTS

This work was supported by the National Natural Science Foundation of China (Grant No. 81625023 and 82104103).

## REFERENCES

- (1) Lu, Z.; Zou, J.; Li, S.; Topper, M. J.; Tao, Y.; Zhang, H.; Jiao, X.; Xie, W.; Kong, X.; Vaz, M.; Li, H.; Cai, Y.; Xia, L.; Huang, P.; Rodgers, K.; Lee, B.; Riemer, J. B.; Day, C.-P.; Yen, R.-W. C.; Cui, Y.; et al. Epigenetic Therapy Inhibits Metastases by Disrupting Premetastatic Niches. *Nature* **2020**, *579*, 284–290.
- (2) Li, J.; Ge, Z.; Toh, K.; Liu, X.; Dirisala, A.; Ke, W.; Wen, P.; Zhou, H.; Wang, Z.; Xiao, S.; Van Guyse, J. F. R.; Tockary, T. A.; Xie, J.; Gonzalez-Carter, D.; Kinoh, H.; Uchida, S.; Anraku, Y.; Kataoka, K. Enzymatically Transformable Polymersome-Based Nanotherapeutics to Eliminate Minimal Relapsable Cancer. *Adv. Mater.* **2021**, *33*, 2105254.
- (3) Zhang, Y.; Jiang, C. Postoperative Cancer Treatments: *In-Situ* Delivery System Designed on Demand. *J. Controlled Release* **2021**, *330*, 554–564.
- (4) Chen, Z.; Zhang, P.; Xu, Y.; Yan, J.; Liu, Z.; Lau, W. B.; Lau, B.; Li, Y.; Zhao, X.; Wei, Y.; Zhou, S. Surgical Stress and Cancer Progression: the Twisted Tango. *Molecular Cancer* **2019**, *18*, 132.
- (5) Liu, Y.; Cao, X. Characteristics and Significance of the Pre-Metastatic Niche. *Cancer Cell* **2016**, *30*, 668–681.
- (6) Wu, J.; Long, Y.; Li, M.; He, Q. Emerging Nanomedicine-Based Therapeutics for Hematogenous Metastatic Cascade Inhibition: Interfering with the Crosstalk between “Seed and Soil. *Acta Pharmaceutica Sinica B* **2021**, *11*, 2286–2305.
- (7) Zhou, Y.; Han, M.; Gao, J. Prognosis and Targeting of Pre-Metastatic Niche. *J. Controlled Release* **2020**, *325*, 223–234.
- (8) Hu, Q.; Li, H.; Archibong, E.; Chen, Q.; Ruan, H.; Ahn, S.; Dukhovlinova, E.; Kang, Y.; Wen, D.; Dotti, G.; Gu, Z. Inhibition of Post-Surgery Tumour Recurrence *via* Hydrogel Releasing CAR-T Cells and Anti-PDL1-Conjugated Platelets. *Nat. Biomed Eng.* **2021**, *5*, 1038–1047.
- (9) Chen, Q.; Wang, C.; Zhang, X.; Chen, G.; Hu, Q.; Li, H.; Wang, J.; Wen, D.; Zhang, Y.; Lu, Y.; Yang, G.; Jiang, C.; Wang, J.; Dotti, G.; Gu, Z. *In Situ* Sprayed Bioresponsive Immunotherapeutic Gel for Post-Surgical Cancer Treatment. *Nat. Nanotechnol.* **2019**, *14*, 89–97.
- (10) Zhao, H.; Song, Q.; Zheng, C.; Zhao, B.; Wu, L.; Feng, Q.; Zhang, Z.; Wang, L. Implantable Bioresponsive Nanoarray Enhances Postsurgical Immunotherapy by Activating Pyroptosis and Remodeling Tumor Microenvironment. *Adv. Funct. Mater.* **2020**, *30*, 2005747.
- (11) Ye, X.; Liang, X.; Chen, Q.; Miao, Q.; Chen, X.; Zhang, X.; Mei, L. Surgical Tumor-Derived Personalized Photothermal Vaccine Formulation for Cancer Immunotherapy. *ACS Nano* **2019**, *13*, 2956–2968.
- (12) Xiang, Y.; Chen, L.; Liu, C.; Yi, X.; Li, L.; Huang, Y. Redirecting Chemotherapeutics to the Endoplasmic Reticulum Increases Tumor Immunogenicity and Potentiates Anti-PD-L1 Therapy. *Small* **2022**, *18*, 2104591.
- (13) Kaufman, H. L.; Kohlhapp, F. J.; Zloza, A. Oncolytic Viruses: a New Class of Immunotherapy Drugs. *Nat. Rev. Drug Discovery* **2015**, *14*, 642–662.
- (14) Liu, Z.; Ravindranathan, R.; Kalinski, P.; Guo, Z. S.; Bartlett, D. L. Rational Combination of Oncolytic Vaccinia Virus and PD-L1 Blockade Works Synergistically to Enhance Therapeutic Efficacy. *Nat. Commun.* **2017**, *8*, 14754.
- (15) Kepp, O.; Marabelle, A.; Zitvogel, L.; Kroemer, G. Oncolysis without Viruses - Inducing Systemic Anticancer Immune Responses with Local Therapies. *Nature Reviews Clinical Oncology* **2020**, *17*, 49–64.
- (16) Krysko, D. V.; Garg, A. D.; Kaczmarek, A.; Krysko, O.; Agostinis, P.; Vandenamee, P. Immunogenic Cell Death and Damps in Cancer Therapy. *Nature Reviews Cancer* **2012**, *12*, 860–875.
- (17) Ye, T.; Li, F.; Ma, G.; Wei, W. Enhancing Therapeutic Performance of Personalized Cancer Vaccine *via* Delivery Vectors. *Adv. Drug Delivery Rev.* **2021**, *177*, 113927.
- (18) Ma, L.; Diao, L.; Peng, Z.; Jia, Y.; Xie, H.; Li, B.; Ma, J.; Zhang, M.; Cheng, L.; Ding, D.; Zhang, X.; Chen, H.; Mo, F.; Jiang, H.; Xu, G.; Meng, F.; Zhong, Z.; Liu, M. Immunotherapy and Prevention of Cancer by Nanovaccines Loaded with Whole-Cell Components of Tumor Tissues or Cells. *Adv. Mater.* **2021**, *33*, 2104849.
- (19) Wang, T.; Wang, D.; Yu, H.; Feng, B.; Zhou, F.; Zhang, H.; Zhou, L.; Jiao, S.; Li, Y. A Cancer Vaccine-Mediated Postoperative Immunotherapy for Recurrent and Metastatic Tumors. *Nat. Commun.* **2018**, *9*, 1532.
- (20) Fang, L.; Zhao, Z.; Wang, J.; Zhang, P.; Ding, Y.; Jiang, Y.; Wang, D.; Li, Y. Engineering Autologous Tumor Cell Vaccine to Locally Mobilize Antitumor Immunity in Tumor Surgical Bed. *Sci. Adv.* **2020**, *6*, No. eaba4024.
- (21) Park, C. G.; Hartl, C. A.; Schmid, D.; Carmona, E. M.; Kim, H.-J.; Goldberg, M. S. Extended Release of Perioperative Immunotherapy Prevents Tumor Recurrence and Eliminates Metastases. *Sci. Transl. Med.* **2018**, *10*, No. eaar1916.
- (22) Song, C.; Phuengkham, H.; Kim, Y. S.; Dinh, V. V.; Lee, I.; Shin, I. W.; Shin, H. S.; Jin, S. M.; Um, S. H.; Lee, H.; Hong, K. S.; Jin, S.-M.; Lee, E.; Kang, T. H.; Park, Y.-M.; Lim, Y. T. Syringeable Immunotherapeutic Nanogel Reshapes Tumor Microenvironment and Prevents Tumor Metastasis and Recurrence. *Nat. Commun.* **2019**, *10*, 3745.
- (23) Liu, J.; Liew, S. S.; Wang, J.; Pu, K. Bioinspired and Biomimetic Delivery Platforms for Cancer Vaccines. *Adv. Mater.* **2022**, *34*, 2103790.
- (24) Li, Y.; Li, L.; Wang, J.; Radford, D. C.; Gu, Z.; Kopecek, J.; Yang, J. Dendronized Polymer Conjugates with Amplified Immunogenic Cell Death for Oncolytic Immunotherapy. *J. Controlled Release* **2021**, *329*, 1129–1138.
- (25) Haug, B. E.; Camilio, K. A.; Eliassen, L. T.; Stensen, W.; Svendsen, J. S.; Berg, K.; Mortensen, B.; Serin, G.; Mirjolet, J.-F.; Bichat, F.; Rekdal, O. Discovery of a 9-mer Cationic Peptide (LTX-315) as a Potential First in Class Oncolytic Peptide. *J. Med. Chem.* **2016**, *59*, 2918–2927.
- (26) Kuai, R.; Yuan, W.; Son, S.; Nam, J.; Xu, Y.; Fan, Y.; Schwendeman, A.; Moon, J. J. Elimination of Established Tumors with Nanodisc-Based Combination Chemoimmunotherapy. *Sci. Adv.* **2018**, *4*, No. aao1736.
- (27) Li, L.; Wang, J.; Radford, D. C.; Kopecek, J.; Yang, J. Combination Treatment with Immunogenic and Anti-PD-L1 Polymer-Drug Conjugates of Advanced Tumors in a Transgenic MMTV-PyMT Mouse Model of Breast Cancer. *J. Controlled Release* **2021**, *332*, 652–659.
- (28) Li, L.; Wang, J.; Li, Y.; Radford, D. C.; Yang, J.; Kopecek, J. Broadening and Enhancing Functions of Antibodies by Self-

Assembling Multimerization at Cell Surface. *ACS Nano* **2019**, *13*, 11422–11432.

(29) Li, L.; Li, Y.; Yang, C. H.; Radford, D. C.; Wang, J.; Janat-Amsbury, M.; Kopecek, J.; Yang, J. Inhibition of Immunosuppressive Tumors by Polymer-Assisted Inductions of Immunogenic Cell Death and Multivalent PD-L1 Crosslinking. *Adv. Funct. Mater.* **2020**, *30*, 1908961.

(30) Xiang, Y.; Chen, L.; Li, L.; Huang, Y. Restoration and Enhancement of Immunogenic Cell Death of Cisplatin by Coadministration with Digoxin and Conjugation to HPMA Copolymer. *ACS Appl. Mater. Interfaces* **2020**, *12*, 1606–1616.

(31) Wang, C.; Wang, J.; Zhang, X.; Yu, S.; Wen, D.; Hu, Q.; Ye, Y.; Bomba, H.; Hu, X.; Liu, Z.; Dotti, G.; Gu, Z. *In situ* Formed Reactive Oxygen Species-Responsive Scaffold with Gemcitabine and Checkpoint Inhibitor for Combination Therapy. *Sci. Transl. Med.* **2018**, *10*, No. aan3682.

(32) Ruan, H.; Hu, Q.; Wen, D.; Chen, Q.; Chen, G.; Lu, Y.; Wang, J.; Cheng, H.; Lu, W.; Gu, Z. A Dual-Bioresponsive Drug-Delivery Depot for Combination of Epigenetic Modulation and Immune Checkpoint Blockade. *Adv. Mater.* **2019**, *31*, No. 1806957.

(33) Zhou, M.; Zuo, Q.; Huang, Y.; Li, L. Immunogenic Hydrogel Toolkit Disturbing Residual Tumor “Seeds” and Pre-Metastatic “Soil” for Inhibition of Postoperative Tumor Recurrence and Metastasis. *Acta Pharmaceutica Sinica B*, in press, **2022**.

(34) Samanta, D.; Park, Y.; Ni, X.; Li, H.; Zahnow, C. A.; Gabrielson, E.; Pan, F.; Semenza, G. L. Chemotherapy Induces Enrichment of CD47(+)/CD73(+)/PDL1(+) Immune Evasive Triple-Negative Breast Cancer Cells. *Proc. Natl. Acad. Sci. U.S.A.* **2018**, *115*, E1239–E1248.

(35) Zhou, M.; Luo, C.; Zhou, Z.; Li, L.; Huang, Y. Improving Anti-PD-L1 Therapy in Triple Negative Breast Cancer by Polymer-Enhanced Immunogenic Cell Death and CXCR4 Blockade. *J. Controlled Release* **2021**, *334*, 248–262.

(36) Ma, S.; Song, W.; Xu, Y.; Si, X.; Zhang, D.; Lv, S.; Yang, C.; Ma, L.; Tang, Z.; Chen, X. Neutralizing Tumor-Promoting Inflammation with Polypeptide-Dexamethasone Conjugate for Microenvironment Modulation and Colorectal Cancer Therapy. *Biomaterials* **2020**, *232*, 119676.

(37) Yi, X.; Yan, Y.; Li, L.; Li, Q.; Xiang, Y.; Huang, Y. Sequentially Targeting Cancer-Associated Fibroblast and Mitochondria Alleviates Tumor Hypoxia and Inhibits Cancer Metastasis by Preventing “Soil” Formation and “Seed” Dissemination. *Adv. Funct. Mater.* **2021**, *31*, 2010283.

(38) Zhang, F.; Lu, G.; Wen, X.; Li, F.; Ji, X.; Li, Q.; Wu, M.; Cheng, Q.; Yu, Y.; Tang, J.; Mei, L. Magnetic Nanoparticles Coated with Polyphenols for Spatio-Temporally Controlled Cancer Photothermal/Immunotherapy. *J. Controlled Release* **2020**, *326*, 131–139.

(39) Lin, Y.-X.; Wang, Y.; Ding, J.; Jiang, A.; Wang, J.; Yu, M.; Blake, S.; Liu, S.; Bieberich, C. J.; Farokhzad, O. C.; Mei, L.; Wang, H.; Shi, J. Reactivation of the Tumor Suppressor PTEN by Mrna Nanoparticles Enhances Antitumor Immunity in Preclinical Models. *Sci. Transl. Med.* **2021**, *13*, No. eaba9772.

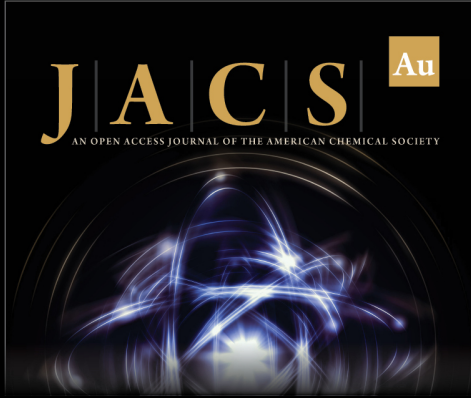
(40) Schroers, B.; Boegel, S.; Albrecht, C.; Bukur, T.; Bukur, V.; Holtstraeter, C.; Ritzel, C.; Manninen, K.; Tadmor, A. D.; Vormehr, M.; Sahin, U.; Loewer, M. Multi-Omics Characterization of the 4T1 Murine Mammary Gland Tumor Model. *Front. Oncol.* **2020**, *10*, 1195.

(41) Zitvogel, L.; Pitt, J. M.; Daillere, R.; Smyth, M. J.; Kroemer, G. Mouse Models in Oncoimmunology. *Nature Reviews Cancer* **2016**, *16*, 759–773.

(42) Boix-Montesinos, P.; Soriano-Teruel, P. M.; Arminan, A.; Orzaez, M.; Vicent, M. J. The Past, Present, and Future of Breast Cancer Models for Nanomedicine Development. *Adv. Drug Delivery Rev.* **2021**, *173*, 306–330.


(43) Shultz, L. D.; Brehm, M. A.; Garcia-Martinez, J. V.; Greiner, D. L. Humanized Mice for Immune System Investigation: Progress, Promise and Challenges. *Nature Reviews Immunology* **2012**, *12*, 786–798.


(44) Li, M.; Li, M.; Yang, Y.; Liu, Y.; Xie, H.; Yu, Q.; Tian, L.; Tang, X.; Ren, K.; Li, J.; Zhang, Z.; He, Q. Remodeling Tumor Immune Microenvironment via Targeted Blockade of PI3K-Gamma and CSF-1/CSF-1R Pathways in Tumor Associated Macrophages for Pancreatic Cancer Therapy. *J. Controlled Release* **2020**, *321*, 23–35.



**JACS Au**  
AN OPEN ACCESS JOURNAL OF THE AMERICAN CHEMICAL SOCIETY

Editor-in-Chief  
**Prof. Christopher W. Jones**  
Georgia Institute of Technology, USA

**Open for Submissions** 

pubs.acs.org/jacsau  ACS Publications  
Most Trusted. Most Cited. Most Read.